Analysis of Red Chalk Drawings from the Workshop of Giovanni Battista Piranesi using Fiber Optics Reflectance Spectroscopy

Maria Krämer (kraemer.papierrestaurierung@googlemail.com)
Stuttgart State Academy of Art and Design https://orcid.org/0000-0002-9128-3194
Ute Henniges
Stuttgart State Academy of Art and Design
Irene Brückle
Stuttgart State Academy of Art and Design
Laura Lenfant
Karlsruhe Institute of Technology Institute of Applied Geosciences: Karlsruher Institut fur Technologie Institut fur Angewandte Geowissenschaften
Kirsten Drüppel
Karlsruhe Institute of Technology Institute of Applied Geosciences: Karlsruher Institut fur Technologie Institut fur Angewandte Geowissenschaften

Research Article

Keywords: fiber optics reflectance spectroscopy, x-ray diffraction, scanning electron microscopy, Giovanni Battista Piranesi, multivariate statistics, principal component analysis, reflectance spectra, red chalk, drawing.

Posted Date: June 3rd, 2021

DOI: https://doi.org/10.21203/rs.3.rs-580566/v1

Abstract

The viability of fiber optics reflectance spectroscopy (FORS) for the differentiation of red chalk drawing media was investigated, focusing on the group of drawings from the workshop of Giovanni Battista Piranesi (1720–1778) at the Staatliche Kunsthalle Karlsruhe, Germany. The evaluation of spectra was supported by principal component analysis. The method was tested on mockup drawings made with recently acquired natural and fabricated red chalks of known origin. It was possible to sort these mockup drawings according to chalk type and application technique. The compositional differences of these reference chalks were confirmed by X-ray diffraction and scanning electron microscopy. Subsequent FORS analysis of selected original drawings revealed the existence of several closely grouped clusters, implying similarities on the basis of the underlying spectral features among the historical red chalks used in Rome. These similarities distinguished the historical drawings from the red chalk mockup drawings, except for the drawings made with red chalk samples from the area near the town of Theley, Germany, which were shown to bear close similarities to those in the cluster of historical samples.

1. Introduction

In this study, we examine the viability of fiber optics reflectance spectroscopy (FORS) as a method for differentiating red chalk drawing media on paper. Our work was carried out in the context of a research project funded by the German Research Foundation (DFG), in which three international partners are studying a group of about 300 drawings at the Staatliche Kunsthalle Karlsruhe (see funding and acknowledgements). These drawings have been reattributed to the Roman workshop of the Italian architect, etcher, and dealer in antiquities Giovanni Battista Piranesi (1720–1778) in 2014 [1, 2, 3]. Among the drawings are many that were executed in natural red chalk. Since this was one of the most versatile drawing mediums used by 18th-century artists, draftsmen, etchers, and architects alike, it is not surprising that it was favored by Piranesi and his circle. Red chalk has a high and varied color intensity and is exceptionally useful in the etcher's workshop for copying and transferring drawings mechanically or via counterproofing. It was a medium for masters in particular, since its strong coloring ability and fine grain precluded erasure and correction.

The Karlsruhe drawings illustrate the rich variety of red chalk tonalities (Fig. 1), ranging from the bright orange prevailing in many 16th-century drawings to the dark reddish tones of the 18th century, found especially in French drawings, as already identified by Meder in 1919 [4 p121]. In the Piranesi workshop, where several different draftsmen were employed and closely cooperated, this wide range of red-chalk tonalities appears in a narrowly defined chronological and geographical context. This makes the drawings an ideal group for the study of variations in color, especially since they were kept undisturbed in albums since the early 19th century. Of special interest in FORS analysis are color variations that result from the compositional differences of the chalks and the additional color variations that result from the artists' application techniques. Smudging, whether intentionally performed, or due to wear, lightens the color; a darker color and a smoother line are produced as a result of oil contact from the tracing of a design, or by the moistening and pressing of a drawing during counterproofing, as has been shown in a

study of the 18th-century artist Daniel Chodowiecki (1726–1801) [5]. These variations are visually differentiable, and can be photographically documented, but those methods are insufficient for the systematic color-oriented comparison of a large number of drawings in numerous collections located far apart from each other. FORS presents an interesting option because it allows rapid measurements, is portable, in our setup was contact-free, and could be used for the comparison of the Karlsruhe drawings with authenticated drawings by Piranesi in other collections.

1.1 Factors influencing color variation in red chalk

Geologically, natural red chalk can be classified as a type of ocher [6 p99]. The hue and intensity of its color result from its mineralogical composition, especially its contents of iron oxides and hydroxides. Reddish ochers primarily contain hematite, Fe_2O_3, whereas goethite, α-FeOOH, is the main Fe-bearing phase in yellowish ochers [7 p70]. The total amount of non-tinting components, such as kaolinite, illite, calcite, gypsum, and dolomite have influence on the lightness of ochers [7]. Natural red chalk from a single mineral deposit can exhibit varying hues and intensities [8 p29], thus artists had a range of tonalities to choose from, even before the advent of fabricated chalks. Morphological differences, including grain size and shape of the Fe oxides and hydroxide crystals, along with their density and presence of impurities in the form of other metal ions, also influence their color appearance. For synthetically produced hematite it has been shown that particle shape and size influences reflection properties: Acicular particles reflect light at higher VIS wavelength ranges more intensively than isometric ones [9; depicted in 10 p135, Fig. 6.12]. Furthermore, the hue of hematite changes from yellowish-red to red-purple as the particle size increases from 0.1 μm to 1.0 μm [11 p57, Fig. 4–1], on to a purplish hue for particle sizes of ~ 1.5 μm [12 p183–184].

Natural red chalk has been found to contain hematite platelets, while fabricated red chalk made from artificial hematite features roundish particles; thus a stronger dependency between particle orientation and color is seen in natural red chalk [13, p176]. This dependency became apparent when field-emission scanning electron microscopy (FESEM) was used to study the effects of red chalk drawing techniques on paper. Wet application resulted in a thick, clumped-up deposit on the paper; dry smudging caused small particles to distribute thinly across the paper surface, with small, iron-rich particles directly attached to the cellulose fibers [6 p110]. Historical sources also indicate that the color of a natural red chalk was manipulated by heating or acid treatment, with varying degrees of success [14 p84, 15 p205].

1.2 Elemental analyses of red chalk and red ocher

Mayer and Vandiver [13 p174, p432] studied hematite and red ocher samples of the Forbes Collection of pigment material, as well as red Conte crayons, using X-ray diffraction (XRD) and scanning electron microscopy (SEM). The samples were composed of 50–80% hematite and 20–50% clay, and quartz. Mayhew et al. analyzed five natural red chalks from different geological sites (in Arizona, Burgundy in France, and three regions in Germany, see Appendix Table A1) using XRD to study their different mineralogical compositions [6 p101–103, see Appendix, Table A1]. In two of the five samples no hematite could be detected. The authors suggested this could be due to the small size of the hematite particles

present, or to their low crystallinity. FESEM revealed natural red chalk strokes on paper to be composed of larger secondary plate-like silicate particles covered by smaller, iron-containing particles, presumably hematite [6 p105–106]. Mößbauer spectroscopy was used to quantify iron-bearing minerals (goethite, hematite, and clay minerals) in ochers from Roussillon, France [16]. Hematite concentrations of 1.5–43.2% were detected in eight of the nine samples. Colored iron compounds in ocher have also been classified using the Munsell Color Charts [17], which are easy to use in field work, and colorimetric methods based on the CIELAB system established by the International Commission on Illumination (commonly known by its French acronym, CIE), a colorimetric system that reproduces human color perception. Both systems utilize data derived from visible (VIS) spectroscopy [7, 16, 17, 18, 19, 20].

In UV-VIS spectroscopy, absorption bands in the reflection or absorption spectrum provide information on the electron transitions taking place in the material. These bands are broad and overlap each other, but they can be amplified and better isolated by calculating derivatives of a spectrum [21]. The color of iron oxide pigments was shown to result from the crystal-field transitions of Fe(III) in an octahedral ligand field [22]. For hematite and goethite, the influence of the ligand-to-metal charge transfer is predominant. It takes place in the UV range, with its absorption edge extending into the VIS range [7 p76]. The electron transfer $2(^6A_1) \rightarrow 2(^4T_1)$ is made possible by the specific shape of the crystal structure of hematite, in particular, by the face-sharing octahedra, which are not found in yellow iron hydroxides. This structural difference is responsible for the shift of the absorption bands toward higher wavelengths, and thus a color shift from yellow to red [22 p1268].

Elias et al. [7] were able to detect a correlation between the a* (redness) coordinate of CIELAB and the position of the inflection point of the steep slope of the VIS reflectance spectrum of ocher samples. The higher the redness value a* and the content of hematite found in the total amount of iron oxides were, the further the inflection point shifted toward the higher wavelengths. The inflection points differed depending on the hues of yellow, orange, and red ochers, with the red ocher accordingly at the highest wavelengths (575–580 nm).The non-tinting constituents of the ochers containing hematite as the main color-forming compound had little influence on the position of the inflection point, but influenced the lightness reading. While earlier studies aimed at analyzing the physical properties of red chalk or understanding the connection between color and composition of ochers, in this study, we aim to explore the viability of FORS-derived spectra in combination with compositional analysis and PCA and better describe similarities and differences of modern and historic red chalk on paper.

2. Experimental Methods And Materials

2.1 Analytical concept

FORS was used on red chalk drawing mockups made with recently acquired natural red chalks (Table 1), and on selected original drawings. The FORS reflectance spectra were analyzed statistically via principal component analysis (PCA). The red chalks were also analyzed with XRD, to quantify their mineralogical composition, and thus, to support the interpretation of the FORS spectra. SEM was used to determine the

elemental composition of the main phases, the distribution of particles in the chalk lines of drawings, and their topography.

2.2 Red chalks studied

Three natural and one fabricated red chalks were used (Table 1). Two types of natural chalks (from German deposits in the area around the town of Theley, Saarland, and the Frankenalb region in Bavaria) were purchased from Kremer Pigments. One additional red chalk sample from the Theley area (sample name “Theley2”) was separately acquired from a private contact person. The fabricated chalk was a Faber-Castell Pitt, No. 122823, made with artificial hematite. Several samples were taken from the chalk pieces for XRD, and FORS readings were taken at several locations on the drawing mockups.

Table 1 red chalk types (n = natural, f = fabricated)

labeling	n/f	image	analysis (see section)	mining origin	supplier
Frankenalb	n		XRD, SEM, FORS	Frankenalb region, in Bavaria	Kremer Pigments
Theley1	n	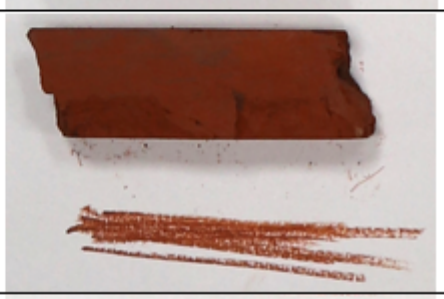	XRD, SEM, FORS	deposits close to the town of Theley, Saarland	Kremer Pigments
Theley2	n		XRD, FORS	see Theley1	private
fabricated	f		XRD, SEM, FORS	artificial hematite	Faber-Castell

2.3 XRD

In order to determine the mineralogical composition of the red chalks, XRD was performed with a D8 Discover instrument (Bruker AXS GmbH), operated at a power setting of 40 kV. Each chalk sample was ground by hand, using an agate mortar. Powder XRD patterns were collected at ambient conditions in the 2Θ range from 2 to 82°, using a step size of 0.02°/2Θ and a counting time of 4 s per step. EVA software (Bruker AXS GmbH) was used for qualitative and semi-quantitative phase analysis. From both natural chalk occurrences, Frankenalb and Theley1, multiple samples acquired between 2014 and 2020 were measured (labeled a, b, c, etc.).

2.4 SEM

The Frankenalb, Theley1, and fabricated red chalks samples were analyzed, using a Tescan Vega 3 instrument. All samples were coated with a nanometer-thick carbon layer, using a Cressington Carbon Coater 108, to increase their electrical conductivity. The chalks' textures were examined in back-scattered electron (BE) mode with an acceleration voltage of 15 kV, mainly in order to identify hematite and rutile. Semi-quantitative analyses of the mineral compositions were conducted with energy-dispersive X-ray spectroscopy (EDX), using an OXFORD INCA x-act instrument, coupled with the SEM. The surface topography of chalk strokes on paper was analyzed mainly in the secondary electron (SE) mode.

2.5 Red chalk drawing mockup preparation

Drawing mockups (Table 2) were prepared with red chalks applied on handmade gelatin-sized rag papers (from here on "historical paper, hp") and handmade gelatin-sized flax papers (acquired from Gangolf Ulbricht, Berlin; from here on "modern paper"). To simulate different artists' drawing techniques, the chalks were applied either dry (a), rubbed (b), wetted (c) or oiled (d, using olive oil; only on modern paper, excluding Theley2, due to effects overlapping with [c]). On each mockup, the chalk was applied in diminishing intensity from high to low coverage (left to right side), to study also the effect of white paper show-through. The chalk application techniques were chosen to simulate the greatest possible range of color variation of a particular red chalk. On aged red chalk drawings, it should be added that application-related differences are most probably diminished, as even smudged chalk lines tend to be compacted and smoothened over time.

Table 2 Red chalk drawing mockups. Circles indicate FORS measuring points. Images are not color-calibrated. (hp) = historic paper

labeling	dry application (a)	smudged (b)	wet application (c)	oiled application (d)
Frankenalb	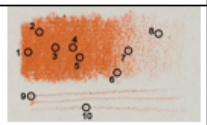	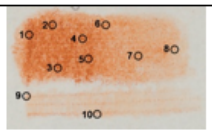	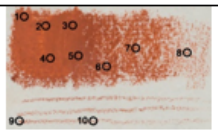	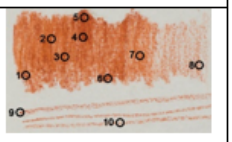
Frankenalb (hp)	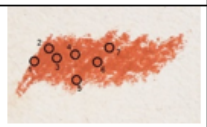	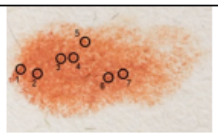	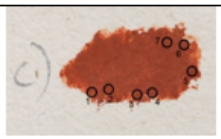	
Theley1	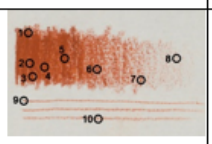	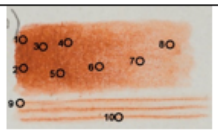	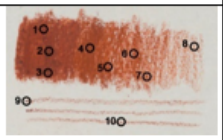	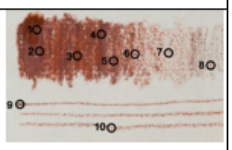
Theley1 (hp)	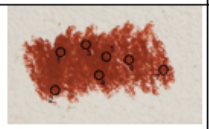	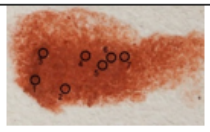	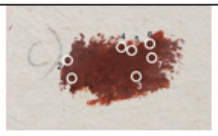	
Theley2	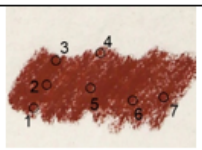	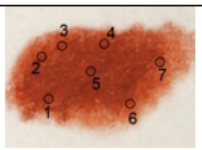	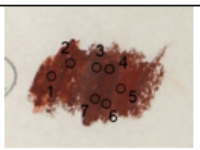	
Theley2 (hp)	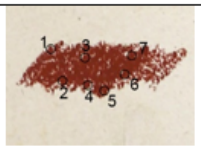	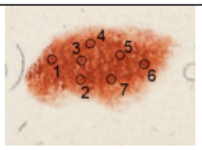	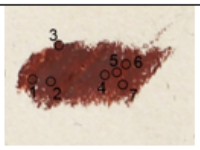	
fabricated	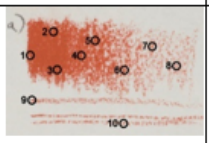	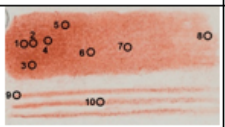	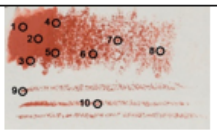	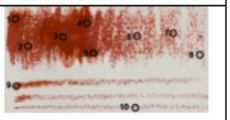
fabricated (hp)	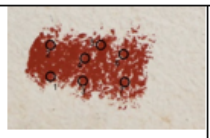	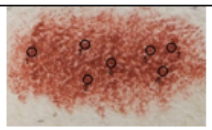	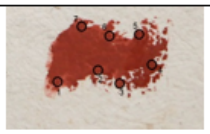	

2.6 FORS: data acquisition

The reflectance spectra were measured using an OceanOptics H2000 + spectrometer with a detection range of 200–1100 nm (detector sensitivity 130 photons/count at 400 nm; 60 photons/count at 600 nm). The light source (DH-2000-BAL) was equipped with a deuterium lamp and a tungsten halogen lamp. Two Zenith Polymer reflectance standards (99% and 2.5% reflectance) were used to calibrate the measurements. The optical fiber heads were fixed in a custom-built frame that enabled contact-free x-y-z

positioning at desired measuring locations. The measuring points were illuminated from two sides at a 45° angle; the measuring head was in the 0° position. During the measurement process, the holder with the fiber heads was covered with a cardboard hood lined with black velvet to exclude ambient light. The integration time fluctuated due to small differences in the insertion of the fiber into the holder. It was adjusted by means of a reflectance standard to conform to 85% (14,000 counts) of the spectrometer's signal capacity before each measurement to improve the replicability of the measurements.

2.7 FORS: CIELAB

CIELAB color values were calculated from the unprocessed FORS spectra via 10° standard observer, D65 illuminant, and at a resolution of 5 nm.

2.8 FORS: Data pre-treatment and PCA

Elias et al. [7] established a relationship between the redness of ochers and the position of the inflexion point of the steep slope in the shorter wavelengths of their VIS reflectance spectra by looking at the first derivative of each spectrum, where the inflexion point is transformed into a maximum. In reference to these findings, several sections of the spectra were analyzed with PCA. The clearest separation of the mockup samples by chalk origin and type was achieved with the wavelength range of 500–650 nm, where the reflection properties of red chalk were consistently measurable even in thin chalk layers.

The FORS spectra were processed and analyzed with the help of a software program (Unscrambler X, Data version 10.5.1; Camo Analytics). Spectra were smoothed, normalized, corrected for multiplicative scattering effects, and the first derivative was computed.

Due to the uneven substrate surface, the contact-free measurement setup, and the instrument’s high level of spectral resolution (Δλ average 0.45 nm), the spectra displayed multiplicative scattering effects and they were also noisy. The spectra were smoothed using the Savitzky-Golay algorithm [23] in the software (61 pts, polynomial order 0). The window adopted for smoothing was relatively large, but since the VIS spectra of red chalks feature broad bands, it was expected that smoothing would not result in the loss of key information.

Several normalization methods and corrections of the scattering effect were compared to each other to investigate their effectiveness and their possible effects on the PCA results. Mean normalization (the division of each spectrum by its average) performed before a multiplicative scattering correction (MSC) yielded the best results. The calculation of the derivative was carried out via the Savitzky-Golay algorithm (61 pts smoothing, second polynomial order). Paper show-through resulted in higher reflectance values at lower wavelength regions with a shortened rise (Fig. 2a). With the first derivative, the spectra from the mix of paper and pigment in the range of 500–650 nm display a weakening and a shift of the maximum in the lower wavelengths (Fig. 2b). Because of this impact on the spectra, only the five measuring points for the most densely-applied strokes were used.

The spectra were further differentiated via PCA. There are various published models for PCA [24, 25]. For our PCA analysis, the singular value decomposition (SVD) for smaller data sets and nonlinear iterative partial least squares (NIPALS) algorithms for complex data sets were used as selected by the software; the validation method was full cross-validation and the data were mean-centered.

3. Results And Discussion

3.1 XRD: Mineral modes of red chalks

All chalk samples are composed of varying proportions of quartz, clay minerals (illite, kaolinite, and/or dickite) and hematite (Fig. 3a; Appendix, Fig. 3b). Additional rutile, TiO_2, is a minor phase in most analyzed samples. Remarkably, the Theley1 and 2 natural chalks contain significantly more hematite and less quartz than the Frankenalb and fabricated chalks. The Theley2 sample additionally contains goethite, which presumably formed at the expense of former hematite during weathering in a near-surface environment. The Frankenalb chalk tends to contain more quartz and clay minerals and significantly less hematite than samples from Theley. In the fabricated chalk, dickite and kaolinite are the dominant clay minerals whereas illite is absent. Quartz contents are remarkably high. The additional presence of corundum in the fabricated chalk is likely attributable to an abrasion of the grinding gear used during production of the chalk sticks. The chalks also display differences with respect to the proportions of amorphous material: The lightest-colored chalk (Frankenalb), which has greater amounts of silicates, shows the highest contents of amorphous material, and the fabricated chalks the lowest. The variability in the mineral modes is generally higher in the natural than in fabricated chalk samples.

3.2 SEM-EDX: Mineral composition, textures and topography of the chalks

3.2.1 Mineralogical composition

The mineral phases of the three chalk types Frankenalb, Theley1, and fabricated, identified via SEM-EDX, correlate well with the XRD results (see 3.1). At high magnifications, it was possible to identify individual mineral grains of quartz and illite, present in variable but mostly highest proportions. Grain sizes are mostly in the micrometer to sub-micrometer range. Minor phases are kaolinite and rutile (Fig. 4). Hematite is present as small platelets, with strongly variable grain sizes, ranging from sub-millimeter up to 5 micrometer.

For each phase, the grain size and amount vary strongly both within individual samples and among different samples. Frankenalb chalk exhibits grain sizes from < 1 µm for the round hematite particles, up to 15 µm for the flaky illite and 10 µm for the kaolinite (Fig. 4a). Theley1 featured only a few large grains (average = 1 µm); overall, it consisted of small, uniform grains that contributed considerably to a closed, compact surface of the chalk stroke (Fig. 4b). In the fabricated chalk sample, angular quartz fragments exhibit a large grain size of up to 20 µm. The sub-rounded hematite and clay mineral particles, in contrast,

are only about 0.5–2 µm in size and homogenously distributed (Fig. 4c). It was not possible to detect an accumulation of hematite in any of the samples.

3.2.2 Effect of smudging on chalk distribution

In all of the red chalk strokes, the mineral particles accumulated along the papermaking fibers on the paper surface. The degree to which the particles were dispersed during smudging varies as a function of the grain form and size, an effect most easily discernible in the areas between the red-chalk strokes. The coarse-grained Frankenalb chalk shows some grains scattered between the chalk strokes, although most of the grains remain where they had been laid down (Fig. 5a). The fine-grained Theley1 shows only a few grains scattered by smudging (Fig. 5b), due to the greater adhesive forces between the small-sized particles. In comparison, the grains in the fabricated red chalk are scattered to the greatest degree (Fig. 5c). The variability of the grain sizes in the sample, with particle sizes of up to 20 µm in diameter, results in significantly lower adhesive forces among the grains.

3.2.2 Effect of wet application on chalk topography

It is evident from the SE images that the wet application method results in a change in the dispersion of the mineral grains. The application of the chalk strokes resulted in a more extensive abrasion of the chalk and therefore thicker coating of the paper. Chalk banks are not – in contrast to the chalk strokes in the dry applications – oriented in the direction of the papermaking fibers. The surface of the chalk strokes of both natural samples, Frankenalb and Theley, is relatively even and massive. A fragile topography is found only in the marginal areas of the chalk applications (Figs. 6a and b). In contrast, the wet application surface of the fabricated chalk is uneven and rough, probably due to the abundant coarse quartz particles (Fig. 6c). These different topographical features of the three red chalks will have a major impact on their lightness and color saturation. Smooth surfaces (e.g., wet chalk strokes) tend to appear darker because they show a greater amount of light reflection than rough (e.g., dry chalk strokes, fabricated chalk) surfaces that show a greater amount of light scattering [26].

3.3 FORS: Spectral features of the red chalk drawing mockups

The four chalk types (see Table 1) show slightly different spectral properties, influenced by their composition, application technique, and the paper support. First, the differences between the types of chalk were observed; for the sake of readability, here they are represented by the median spectra of the dry application on modern paper (Fig. 7). The curve shapes of the reflectance spectra of the red-chalk mockups differ most significantly at the start of the rise at 550 nm, and with respect to the form of the slope of the rise between 600–750 nm, as well as following the second rise, between ca. 760–950 nm (indicated by arrows).

The red chalk types could not be divided into groups solely based on the values for the maximum in the first derivate, even though trends were identified (Fig. 8a; breakdown regarding application technique and chalk type, see Fig. 8b in the Appendix). The peak heights and positions for the natural chalks were found to be similar, and in general, they were more widely dispersed than those of the fabricated chalks; the latter tend to display higher values with respect to these two points, with the smallest variation in the peak shift. The shift in the peak of the first derivative was overall quite small and occurred between 577 nm and 589 nm. With our samples, there was no link between the hematite content and the position or the height of the maximum, as implied by studies using mixtures of synthetic sediments and very minor parts (up to 1%) of hematite and goethite [17 p631]. The shift induced by application technique was greater than that which was induced by compositional differences of the chalk type. In samples with a lower maximum, this maximum tends to move towards the higher wavelengths (see Fig. 8b, Appendix). All of the wet and oiled chalk applications have lower peaks at higher wavelengths, whereas all of the dry and smudged applications have higher peaks at lower wavelengths. The fabricated red chalk with synthesized hematite was the only sample that displayed notably higher maximum readings. The production process of this chalk, optimized for color brightness and a more homogeneous product, assumedly could explain this.

The form of the first derivative of the spectra differed in accordance with the type of chalk and bundled sufficiently to facilitate their classification using PCA. The spectral curves could be best distinguished in the measurements taken from the smooth and dense applications of wet chalk strokes (Fig. 9a; other applications, see Figs. 9b–d in the Appendix).

The shape of the spectral curves was also influenced by the chalk application technique (dry, smudged, wet, and oiled), as illustrated for the Theley1 measurements (Fig. 10a; other chalks, see Figs. 10b–d in the Appendix). Compared to the dry chalk strokes, the ones compacted by wetted or oiled application shifted the first slope rise towards higher wavelengths (see left arrow), and increased the absorption maximum in the near-infrared range (see right arrow). The spectra of the smudged chalks that featured more paper show-through displayed a steeper slope rise that started at lower wavelength (ca. 610 nm) and flattened out at 750 nm with a lower minimum in the subsequent higher area.

The paper type has an effect primarily on the dry and smudged red chalk samples, which can probably be attributed to the paper partially showing through the chalk. The blank modern paper features a higher reflectance in the low nm range than the blank historical paper, and a lower reflectance in the high nm range (Fig. 11). As can be expected, these trends influence the spectral curves of the dry chalk applied to the two papers. In the first derivative, the historical paper, in contrast to the modern paper, tends to give rise to a lower peak with a shift at higher wavelengths in the dry application types.

3.4 FORS: Interpretation of FORS spectra on the basis of CIELAB

The visual color perception of the red chalk mockups can be expressed in CIELAB values (Fig. 12).

Based on this system, it is possible to detect differences between the red chalk types. The Frankenalb chalk exhibits overall high L*a*b* values. They scatter less than the Theley chalks, which show the greatest variance and the lowest values for all three color properties of all the chalk types, caused by oiled and wet applications. The notable differences in hematite content cannot be seen expressed in the a*-values. As other research groups studying hematite-deferrated soil mixtures have shown [27], this could be due to amounts of hematite close or above a saturation point (10%), where only little fluctuation in color can be observed. However, the hematite-rich Theley samples exhibit readings with clearly lower L*a*b*-values than the other two samples and therefore appear darker and less saturated. It is notable that a higher content of non-tinting minerals are indicated by higher trending L*-values for the Frankenalb and fabricated red chalks. It is possible that, at these high hematite concentrations, other factors (topography, particle shape) have stronger influence on the color appearance of red chalks than the hematite content. The fabricated chalk shows the least scattering which can be explained by its homogeneous composition (see 3.1 and 3.2). The greatest variation between the color values, however, can be explained by the different application techniques. Within each of the chalk types, the measuring points for the dry and smudged application techniques tend to have higher L*a*b* values than those for the wet and oiled applications.

3.5 Principal component analysis of red chalk mockups

For all chalk application techniques and paper types, PCA sorts the chalks into well-defined clusters in keeping with the chalk type (Fig. 13). Overall, three principal components explain 99% of the variance, whereby PC-1 explains 58%, but PC-2 and PC-3, taken together, still explain a significant amount, namely 41% of the variance. The Theley1 and Theley2 chalks, which stem from the same geological area, make up one point cloud. The differences between these two and the two other chalk types are represented primarily in PC-2 and PC-3. The fabricated chalks showed more pronounced clustering than the natural red chalks, indicating lower variance of surface topography within this red chalk type.

Within each group, the measuring points are dispersed in an elongated point cloud, sorted by the chalk application technique. The points spread along the axis of PC-1, which explains most of the variance. The dry chalk applications can, to an extent, be differentiated from the wet chalk applications. It is also possible to distinguish the applications on historical paper (the unfilled symbols) from the samples on modern paper.

The loadings plot (Fig. 14a) was used to interpret the scores plot. It shows which wavelength ranges of the first derivative have an impact on the scores for each PC. In sum, PC-1 indicates differences in peak height (Fig. 14b in the Appendix), PC-2 differences in peak width and PC-3 differences in peak position (Fig. 14c in the Appendix).

For PC-1, the loadings plot, which followed the curve shape of the first derivative, showed that values around the maximum (at about 570 nm) of the investigated wavelength range had the greatest impact: Samples with positive PC-1 scores in these areas had higher than average values. This value is directly related to the chalk application technique: For PC-1, the chalk strokes with rough surface (dry) or low

coverage (smudged) showed the highest values, and the chalk applications that were compact and featured high coverage show the lowest values. Where the loadings plot for PC-1 showed a maximum, the loadings plot for PC-2 described a minimum in the negative region of the y-axis, slightly shifted toward the higher wavelengths (at 584 nm). The loadings plot curve intersects the x-axis at 564 nm and at 603 nm. There are two maxima, one at 545 nm, and one at 623 nm, whereby the maximum in the higher wavelength range has a higher impact on the PC-2 scores than the lower one. The two maxima in the PC-2 loadings plot mark differences in the width of the first derivative's maxima of the samples. High impact loadings values in those ranges next to the actual maximum in the first derivative make it possible to describe the width of the curve, which was the important attribute for the determination of the chalk type in the analysis of the mockups. In the loadings plot for PC-3, the maximum from the loadings plot for PC-1 describes the curve's point of inflection (at 578 nm). The reflectance values before that point positively correlate with PC-3, with a maximum at 553 nm, and the values after that point correlate negatively, with a minimum at 604 nm. Thus, PC-3 explains differences in the peak position. The higher the wavelength range of the maximum, the lower the value is for PC-3. Variances in the FORS spectra that could be visualized with PCA are also reflected in the CIELAB values. PC-1 correlates directly with the chromaticity values of the same measuring points and to a lesser degree with the lightness values: The higher the CIELAB values, the higher the PC-1 values (Fig. 14d in the Appendix).

Since it was also possible to determine the impact of the application technique and paper type within a particular chalk, these factors were subjected to PCA analysis with the exclusion of other factors (that is to say, all of the application techniques for one chalk type on the same paper; or both paper types with the same application type and chalk type; or different types of chalk on the same paper type and with the same application technique). In all cases, 95% of the variance could be expressed with only two principal components, and often the share contributed by PC-1 alone amounted to more than 90% of the variance. This implies that a sole factor accounts for most of the differences.

In most of the samples, it was possible using PCA to identify slight differences for a single chalk type on the basis of the application technique and the paper support. The differentiation of the application technique occurred primarily between dry and wet drawing techniques, in the positive and negative regions of PC-1 (Fig. 15a, see also Figs. 15b–d in the Appendix). In three cases, groups formed loosely based on the chalk application technique. It was also possible to differentiate the paper a type wherever their show-through was a contributing factor in the measurements; however, in two cases the effect falls within the differentiation axes of PC-2, with an explained variance of 9–18%. It is thus possible for PCA to analyze differences in the application type or paper for a single red-chalk type and thereby cause "false positive" results.

3.6 Differentiation of the red chalks in the Karlsruhe drawings

FORS measurements of 79 red-chalk drawings were taken and analyzed using PCA to group them according to their spectral similarity. This allows drawing conclusions about the diversity of the red

chalks used in the Piranesi workshop and in Rome. For drawings with more than 10 measured spectra, in each case the 10 spectra with maximum values closest to the median of the maximum values in the first derivative were used, to exclude outliers. In these cases, it was assumed that only one type of red chalk was used per drawing. For individual drawings, however, it should be considered that outliers might point toward different chalk types used on the same drawing.

The positions of the peaks in the first derivatives of the average spectra of the historic red-chalk samples were found between 571 and 589 nm, and the height was between 0.00305 and 0.00658 (Fig. 16). The spectra of the historical samples resemble mostly those from Theley.

In the loadings plot, PC-1 describes the peak height of the spectra in the first derivative, PC-2 correlates with the peak position, and PC-3, which accounts for 6% of the variance, shows differences in the width of the curve, which is the main differentiating factor among the red chalks in the mockups (Fig. 17a). Plotting the principal components with CIE L*a*b* values (Fig. 17b in the appendix) supports this interpretation. PC-1 correlates with the a* and b* values of the historic drawings, i.e., red and yellow (Fig. 17c in the Appendix). The L* value correlates with the peak position and tends to be projected onto PC-2 (Fig. 17d in the Appendix). A high PC-2 value indicates there is a particularly light color and that the position of the maximum is found in the lower wavelengths.

In the PCA score plot (Fig. 18a–c; 2D scatter plots see Fig. 18d-f in the Appendix) the measuring points in the aggregate constitute a large, coherent point cloud, in which the respective drawings each take up clearly located and distinctly demarcated sub-spaces; individual drawings, however, exhibit more extensive scattering. The combined point cloud for all the drawings can be clearly differentiated from the clouds for the Frankenalb red chalk and the fabricated red chalk, but the measuring points of the aggregate cloud lie close to the elongated point cloud of the Theley chalks. The measuring points for the Frankenalb, Theley1 and Theley2 and Faber-Castell chalks are concentrated in the positive region of PC-1, and primarily in the negative region of PC-2. PC-3 is needed to separate the mockups into groups in regards to their chalk types. In an attempt to interpret the score plot based on the greatest overlaps; groups of same-colored symbols were assigned to the historical drawing measurements, which consisted of red-chalk drawings that were the most similar to each other. At the negative end of PC-1, there is a clear overlapping of the measuring points from several drawings, which cluster and form a compact group (violet symbols). Set apart from this group, a second (beige symbols) forms, slightly offset toward the right on PC-1, and displaying a clear shift on PC-3. Some of the drawings from these two groups could also be connected regarding their historical use and content, through the identification of several counterproofs that were made from them for architects visiting Rome, and which at present are attributed to the French draftsman Nicolas François-Daniel Lhuillier [1]. Counterproofing a freshly made drawing involved moistening it, which was advantageous because it fixed the remaining media on the paper, thereby prevented loss and smudging [5]. This facilitates the characterization of the chalks, as expressed in a lesser degree of data scattering, and a clear gab between their respective clusters. The red chalks that are not as easy to characterize are found in the center of the PC-1 scale. Their data points have a greater tendency to scatter, and they cannot be assigned to a compact overall group (symbols in pink, purple,

green and other colors). Yellow symbols mark red-chalk drawings featuring a low coverage with paper show-through, which also scattered to a great degree toward PC-2. At the positive end of PC-1 of the point cloud of historical red chalk samples, a number of red chalks, in turn, clearly overlap each other (red symbols).

We chose selected original drawings (Fig. 19a) to show how differences in the reflectance spectra and the first derivative (Figs. 19b–c) impact the score plot. Red chalks with negative PC-1 values (beige and violet symbols) display a flatter spectrum with higher initial reflectance values (35-13-1 in Figs. 19b–c). The chalks on the positive end of PC-1 (in red) are characterized by the steeper rise of their spectra with lower initial reflectance values (35-10-2 in Figs. 19b–c). The chalks in the middle of PC-1 that have distinctly positive values for PC-2 have a spectrum with a similarly steep slope, but markedly higher initial reflectance values. In the first derivative this feature is expressed as a high peak accompanied by a shift of the maximum into the lower wavelength regions; this correlation was observed for the mockups, in connection with applications that featured lower coverage or smudging.

4. Conclusion

PCA enhances the comparison of spectral data of different substrates and clusters them accordingly. To interpret the PCA results, the specific factors that influence them need to be linked to the individual differences in the spectra. In this study, the interpretation of the red chalk spectra is based on known differences of the mock-up preparation (different chalk types, paper supports, and application techniques) and analysis of the mineral composition of the chalks studied.

Four different natural and fabricated red chalk reference samples could be differentiated based on their FORS spectra via PCA, which indicates the potential of FORS in the differentiation of red chalks on original drawings. We could show that chalk composition and the application technique on paper influence the VIS spectra. These variations are expressed through different spectral shapes and CIELAB color values. Via PCA, it is possible to visualize these differences based on a selected region (500–650 nm) of the VIS spectrum in the first derivative. For the red chalk drawings of the Karlsruhe Piranesi albums, PC-1 correlates with the CIE a* and b* values of the chalks, i.e., their redness and yellowness. The L* value correlates with the position of the maximum in the first derivative and tends to be expressed in PC-2, thus a high PC-2 value indicates a particularly light color.

FORS measurements of art on paper will be influenced by the unevenness of the paper support. In the context of required non-contact measurements on historic objects, this leads to a greater variance within the spectra. This should be compensated for with a multiplicative scattering correction. In addition, the degree of coverage within a red chalk line has an influence on the interpretation of the data. These factors can lead to ambiguities in the interpretation of the PCA, therefore a compositional analysis must accompany a study that seeks to differentiate between red chalk types. FORS in combination with PCA cannot provide information about the origin of a chalk since this information is reflected primarily in the colorless components of the chalk and its chemical composition, including trace elements.

When this analytical concept was applied to a large group of red-chalk drawings from the Piranesi workshop, it was also possible to identify differences among the individual drawings. These, however, could not be clearly attributed to a single factor, e.g., hematite content. Despite these limitations of FORS in the study of red chalk as one single drawing medium, it was possible via PCA to divide up the historical red chalks that had a close temporal and spatial relationship to each other into several groups. The distances between the groups were considerably smaller than those between the original samples and the mockup chalks, and all samples together were spread across a range in which two red chalk mockups from one geological region (Theley1 and 2) were represented.

By using a larger range of comparison spectra from known sample chalks, it may be possible to further refine the differentiation of the PCA. In combination with multivariate analysis, FORS can thus become a powerful tool for the contactless differentiation of single drawing media. Another question to be studied in this connection could be the differentiation between fabricated and natural red chalks, for which promising approaches have been described in this paper. As the use of natural red chalk steadily declined during the 19th century with the production of synthetic hematite pigments (so-called “Mars Colors”) [13, p178], combining FORS and PCA could also be helpful in the detection of forgeries.

5. Abbreviations

BE: Back-scattered electron

CIE: Commission Internationale de l'Éclairage (International Commission on Illumination)

DFG: Deutsche Forschungsgemeinschaft (German Research Foundation)

EDX: Energy-dispersive X-ray spectroscopy

FESEM: Field-emission scanning electron microscopy

FORS: Fiber optics reflectance spectroscopy

NIPALS: Nonlinear iterative partial least squares

PCA: Principal component analysis

SE: Secondary electron

SEM: Scanning electron microscope

SVD: Singular value decomposition

XRD: X-ray diffraction

6. Declarations

Availability of data and materials

The datasets analyzed during the current study are available from the corresponding author upon reasonable request.

Competing interests

The authors declare that they have no competing interests.

Funding

The project “Giovanni Battista Piranesi and his workshop: Two Newly Identified Albums in Karlsruhe“, to which this research contributes, is funded by the German Research Foundation and the Swiss National Science Foundation (DFG, project number 323516160; https://gepris.dfg.de/gepris/projekt/323516160 and SNSF project numbers 170303 and 185525; http://p3.snf.ch/project-170303 and http://p3.snf.ch/project-185525, accessed 9 May 2021).

Contributions

MK was responsible the conception of the study. She carried out the FORS analysis, was responsible for the realization and interpretation of the PCA, and for drafting and revising the manuscript. UH suggested PCA and supported the analysis, the spectral data interpretation and management, as well as editing the manuscript. LL and KD provided the SEM and SEM-EDX analyses and data interpretation, carried out the XRD analysis, and provided mineral modes and interpretation of the mineralogical data. Critical editing of the manuscript was provided by IB. All authors read and gave their approval of the final manuscript.

Acknowledgements

The DFG is gratefully acknowledged for making this research possible. We also thank Tiziana Cavaleri at the Fondazione Centro Conservazione e Restauro "La Venaria Reale" Turin for valuable information on the practice of FORS, computation and interpretation of data, and for supporting measurements. Her input in the initial phase of the project was vital in setting us on the path that led to this paper. We also would like to thank Dorit Schäfer at the Kunsthalle Karlsruhe for her instrumental and continued support in the Piranesi research project. We thank Johannes Gfeller, director of the study program New Media and Digital Technology at the Stuttgart State Academy, who engineered and built the FORS measuring frame and Natascha Wichmann for initial testing of FORS with the custom-built system as part of student projects at the Stuttgart State Academy (see Krämer).

7. References

1. Kabierske G. A cache of newly identified drawings by Piranesi and his studio at the Staatliche Kunsthalle Karlsruhe. Master Drawings. 2015;53:147–78.
2. Kabierske G. Weinbrenner und Piranesi. Zur Neubewertung von zwei Grafikalben aus dem Besitz Friedrich Weinbrenners in der Staatlichen Kunsthalle Karlsruhe. In: Kleinmanns J, Baumstark B, editors. Friedrich Weinbrenner 1766–1826, Architektur und Städtebau des Klassizismus. Petersberg: Imhof; 2015a. pp. 75–87.
3. Kabierske G, Vasi. urne, cinerarie, altari e candelabra: newly identified drawings for Piranesi's antiquities and sculptural compositions at the Staatliche Kunsthalle Karlsruhe. In: Nevola F, editor. Giovanni Battista Piranesi. Predecessori, contemporanei e successori: studi in onore di John Wilton-Ely. Vol. 32. Rome: Edizioni Quasar; 2016. pp. 245–62., (= Studi sul Settecento romano.
4. Meder J. Die Handzeichnung – ihre Technik und Entwicklung (2nd edition). Wien: Scholl&Co; 1923.
5. Glück E, Krämer M. Chodowieckis Rötelzeichnungen für das plastische Bildprogramm des Französischen Doms in Berlin – Kunsttechnologie und Restaurierung. In: Schultz A, editor. Turmbewohner. Entwurfszeichnungen von Chodowiecki und Rode für den Gendarmenmarkt. Berlin: Akademie der Künste; 2014. pp. 71–87.
6. Mayhew TD, Hernandez S, Anderson PL, Seraphin S. Natural red chalk in traditional old master drawings. JAIC. 2014;53(2):89–115.
7. Elias M, Chartier C, Prévot G, Garay H, Vignaud C. The colour of ochres explained by their composition. Materials Science Engineering: B. 2006;127(1):70–80. https://doi.org/10.1016/j.mseb.2005.09.061.
8. Reissland B. Puur natuur. Rood tekenkrijt in de geschiedenis. Tijdschrift van de Rijksdienst voor het Cultureel Erfgoed. 2019;2:28–30.
9. Hund F. Inorganic pigments: Basis for coloured, uncoloured and transparent properties. Angew Chem Int Ed Eng. 1981;20:723–30.
10. Cornell RM, Schwertmann U. The Iron Oxides: Structure, Properties, Reactions Occurrences and Uses. 2nd edition. Weinheim: Wiley-VCH; 2003.
11. Schwertmann U. Relations Between Iron Oxides, Soil Color, and Soil Formation. In: Bigham JM, Ciolkosz EJ, editors. Soil Color (Vol. 31). 1993. p. 51–69. https://doi.org/10.2136/sssaspecpub31.c4.
12. Kerker M, Scheiner P. Cooke DD, Kratohovil JP. Absorbance index and colour of colloidal hematite. J Colloid Interface Sci. 1979;71:176–87.
13. Mayer DD, Vandiver P. Red Chalk: Historical and Technical Perspectives. Part 2: A Technical Study. In: Strauss W, editor. Drawings Defined. New York: Abaris Books; 1987. pp. 171–80. Suppl p. 432.
14. Reinhold CL. Die Zeichen- und Mahlerschule. Münster: Phillip Heinrich Perrenon; 1786.
15. Church AH. The chemistry of paints and paintings. London: Seeley, Service&Co. limited; 1915.
16. Dubiel S, Cieslak J, Tarasiuk J, Niziol J. Relationship between colours of ochre from Roussillon and content of iron-bearing minerals. Appl Clay Sci. 2011;51(1–2):54–60. https://doi.org/10.1016/j.clay.2010.11.001.

17. Deaton BC, Balsan WL. Visible spectroscopy. A rapid method for determining hematite and goethite concentration in geological materials. J Sediment Petrol. 1991;61:628–32.
18. Fernandez RN, Schulze DG. Munsell colors of soils simulated by mixtures of goethite and hematite with kaolinite. Zeitschrift für Pflanzenernährung Bodenkunde. 1992;155:473–8. https://doi.org/10.1002/jpln.19921550520.
19. Scheinost A, Chavernas A, Barrón V, Torrent J. Use and limitations of second-derivative diffuse reflectance spectroscopy in the visible to near-infrared range to identify and quantify Fe oxides in soils. Clays Clay Miner. 1998;46:528–36. https://doi.org/10.1346/CCMN.1998.0460506.
20. Scheinost A, Schulze D, Schwertmann U. Diffuse reflectance spectra of Al substituted goethite: A ligand field approach. Clays Clay Miner. 1999;47:156–64. https://doi.org/10.1346/CCMN.1999.0470205.
21. Huguenin RL, Jones JL. Intelligent information extraction from reflectance spectra: Absorption band positions. J Geophys Res. 1986;91:9585–98.
22. Sherman DM, Waite TD. Electronic spectra of Fe3 + oxides and oxide hydroxides in the near IR to near UV. Am Miner. 1985;70(11–12):1262–9.
23. Savitzky A, Golay MJE. Smoothing and differentiation of data by simplified least squares procedures. Anal Chem. 1964;36:1627–39. doi:10.1021/ac60214a047.
24. Jackson JE. A User's Guide to Principal Components. New Jersey: John Wiley & Sons; 1991.
25. Vidal R, Ma Y, Sastry SS. Generalized Principal Component Analysis. Interdisciplinary Applied Mathematics 40. New York: Springer; 2016.
26. Simonot L, Elias M. color change due to surface. state modification. Color Research Application. 2003;28:45–9. doi:10.1002/col.10113.
27. Barrón V, Torrent J. Use of the Kubelka—Munk Theory to Study the Influence of Iron Oxides on Soil Colour. J Soil Sci. 1986;37:499–510. doi:10.1111/j.1365-2389.1986.tb00382.x.

Figures

Figure 1

Two leaves of the Karlsruhe Albums, showing a selection of the red chalk drawings (Staatliche Kunsthalle Karlsruhe, folios 9 (left) and 10 (right) of Volume 1, Inv.-No. IX 5159-35); photographs: Annette T. Keller.

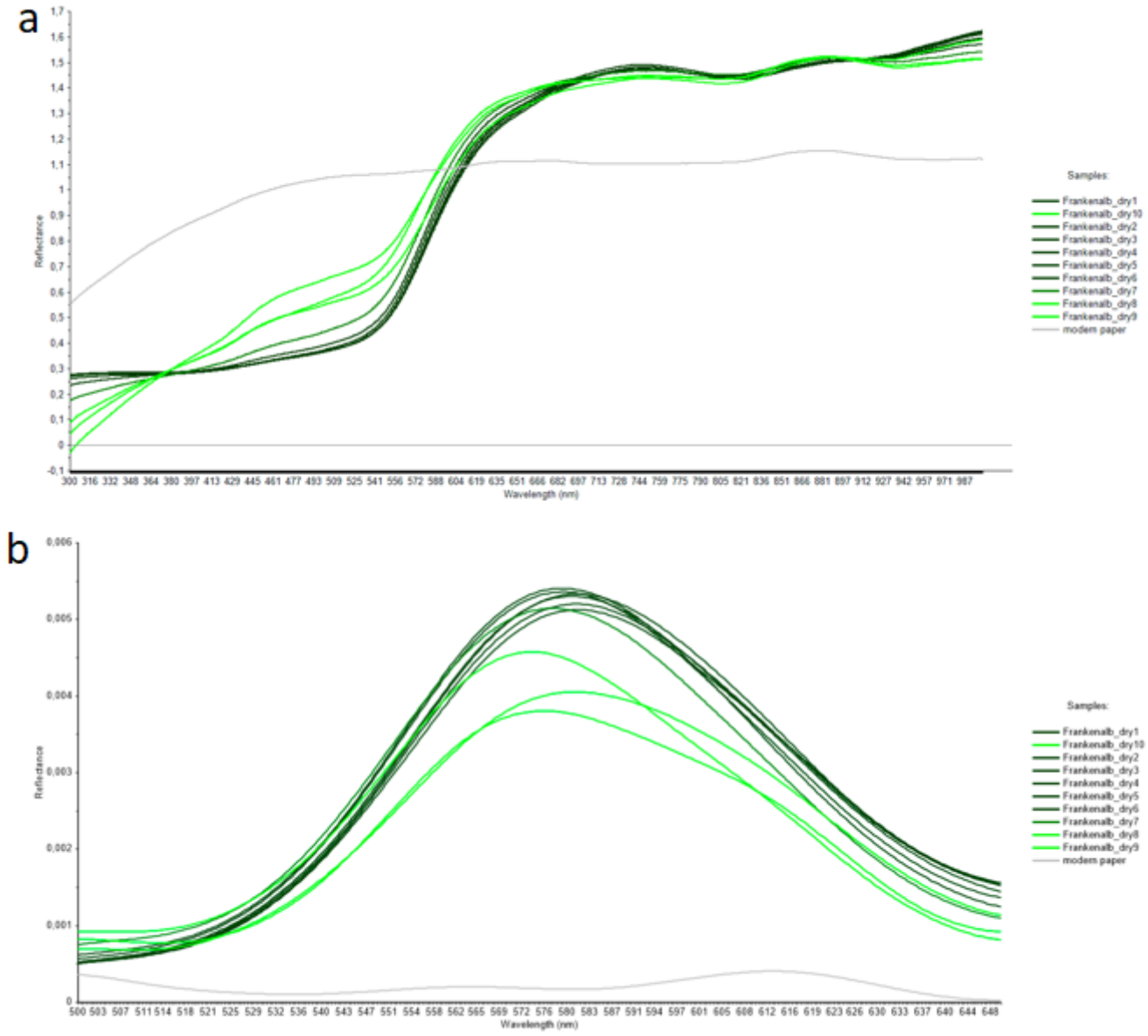

Figure 2

a–b: a: FORS spectra (normalized and corrected for multiplicative scattering effects) of dry Frankenalb red chalk applied in high (dark green) or low (light green) intensity on modern paper (gray); b: 1st derivative of the spectra between 500–-650 nm, showing the formation of a shoulder resulting from paper show-through.

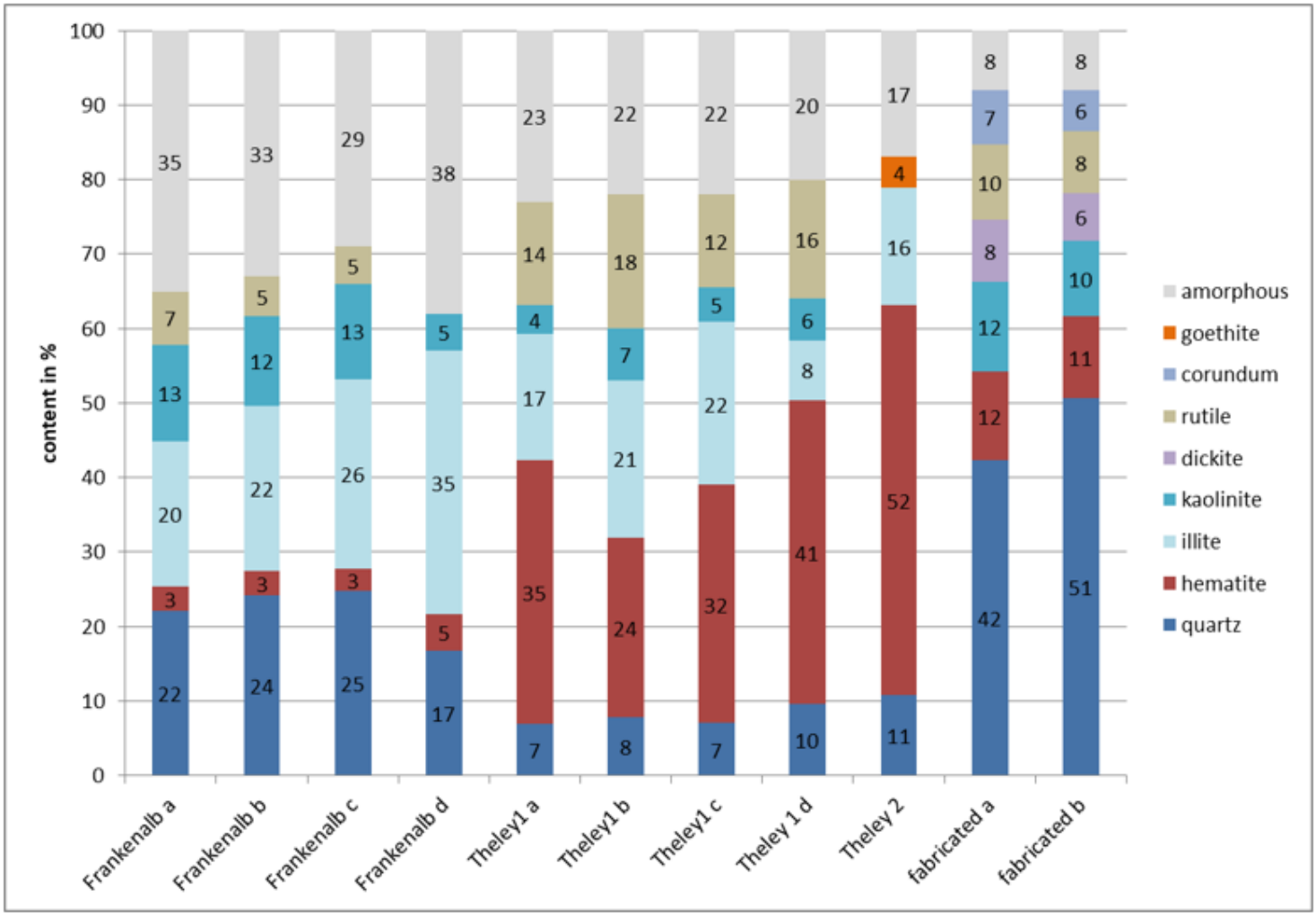

Figure 3

a: Mineralogical composition of red chalks, determined via powder XRD. Letters (a, b, c, d) indicate multiple samples/readings of different batches of the same chalk type, samples acquired between 2000 and 2014.

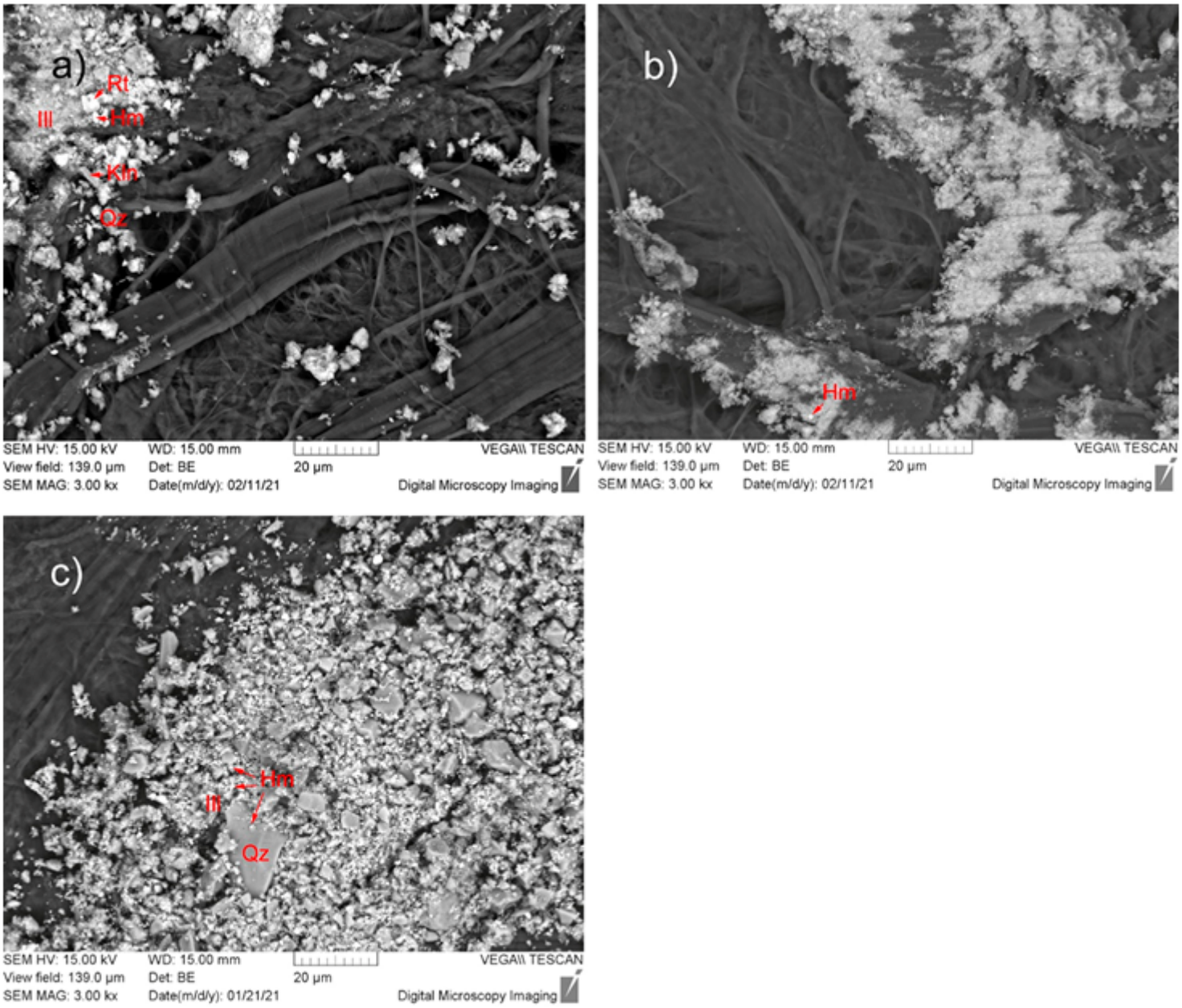

Figure 4

a–c: SEM images (BSE mode) of red chalk applied dry on paper: Frankenalb (a), Theley1 (b) and fabricated (c). The white particles consist mainly of hematite and minor rutile. The gray particles include illite, kaolinite, and quartz (Hm: hematite, Ill: illite, Kln: kaolinite, Qz: quartz, Rt: rutile)

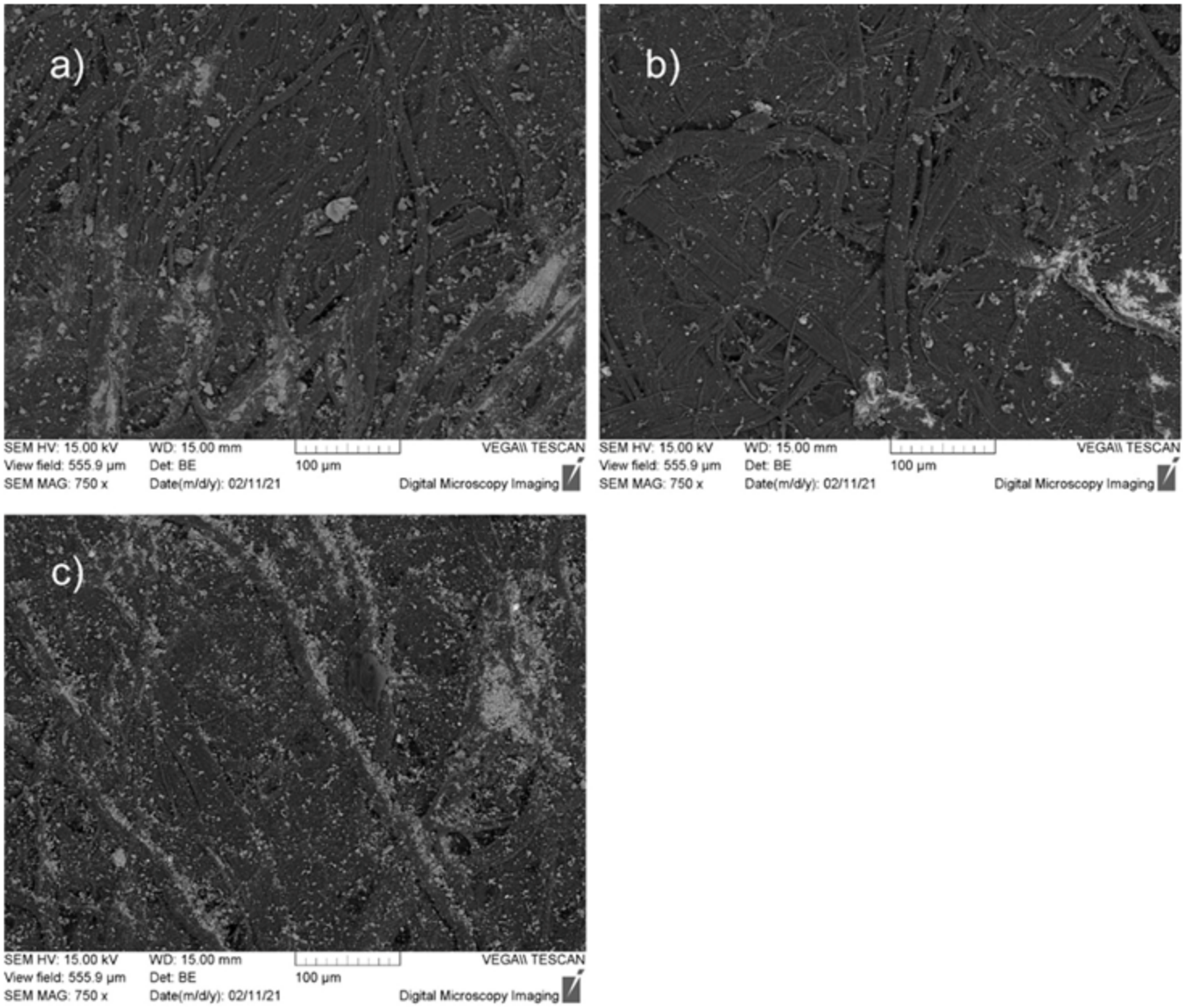

Figure 5

a–c: SEM images (BE mode) of smudged red chalk strokes on paper: Frankenalb (a), Theley1 (b), and fabricated (c). The chalk mineral grains are finely dispersed and scattered across the paper surface to various degrees, depending on grain size and shape: (b) finest grains with the least amount of scattering; (c) coarsest grains, largest amount of scattering, with particles accumulating in the valleys between fibers.

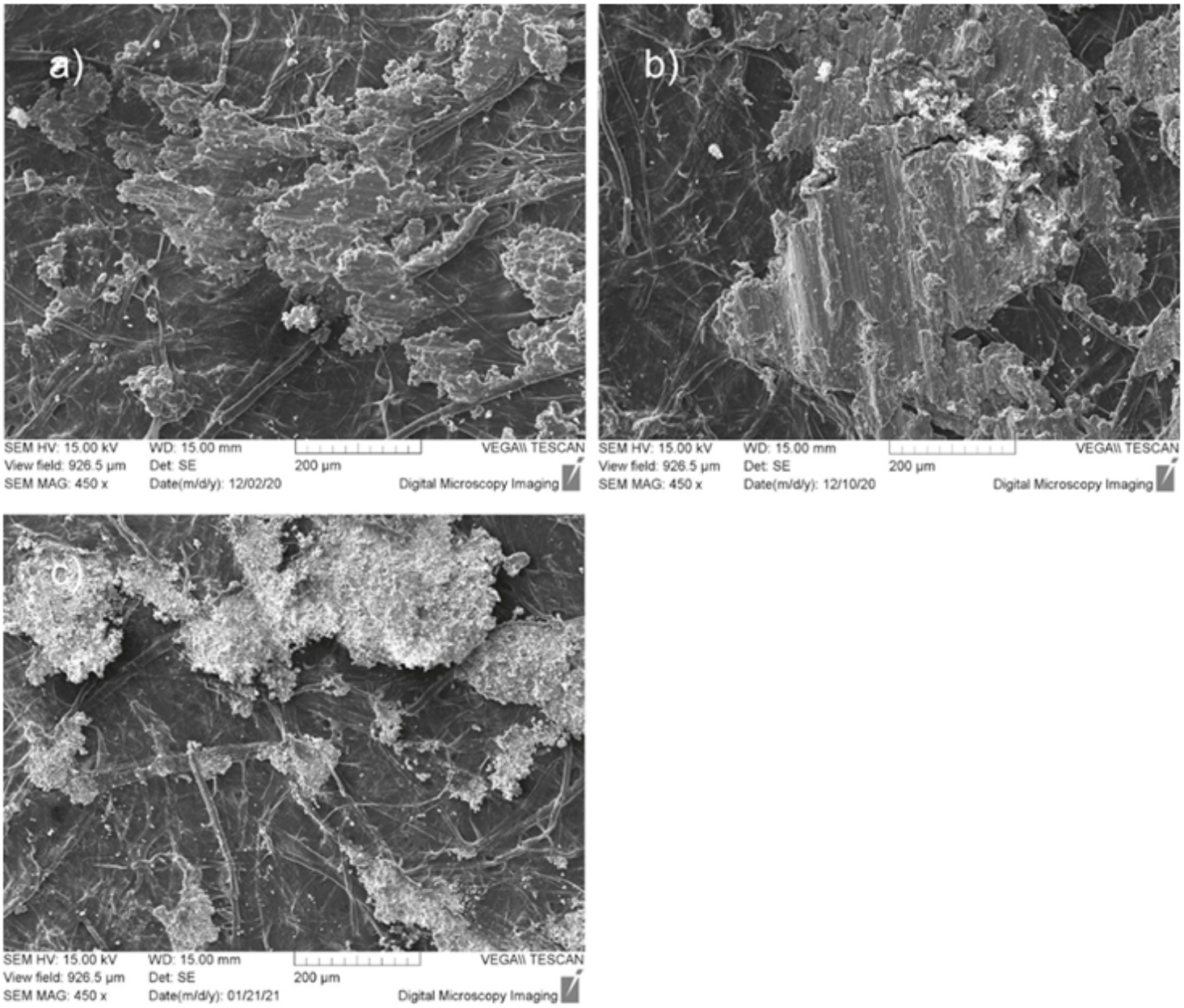

Figure 6

a–c: SEM images (SE mode) of red chalks applied wet on paper: Frankenalb (a), Theley1 (b), and fabricated (c). The chalk strokes form thick layers that coat the paper surface. Moisture-induced caking results in diminished surface roughness, which is observable to a greater extent in the natural chalks than the coarse-grained fabricated chalk.

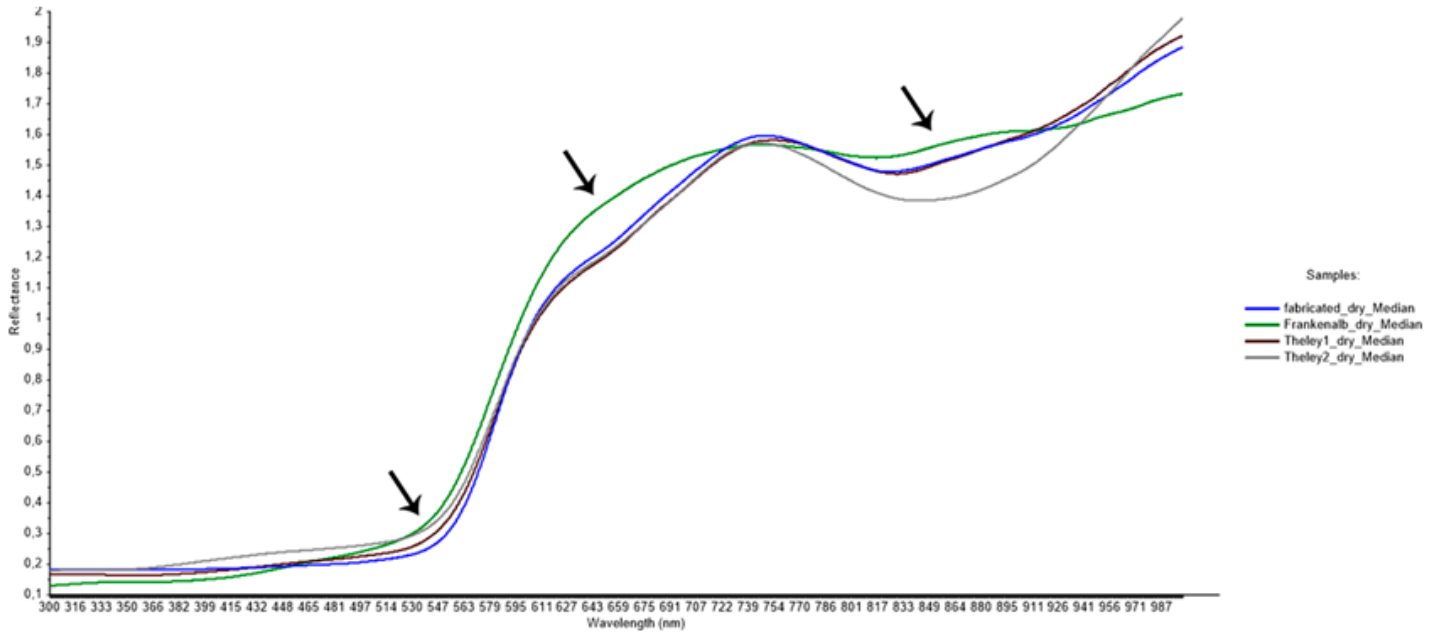

Figure 7

Median FORS spectra for all chalk types (Table 1) applied dry on modern paper. Arrows mark areas with most significant variance.

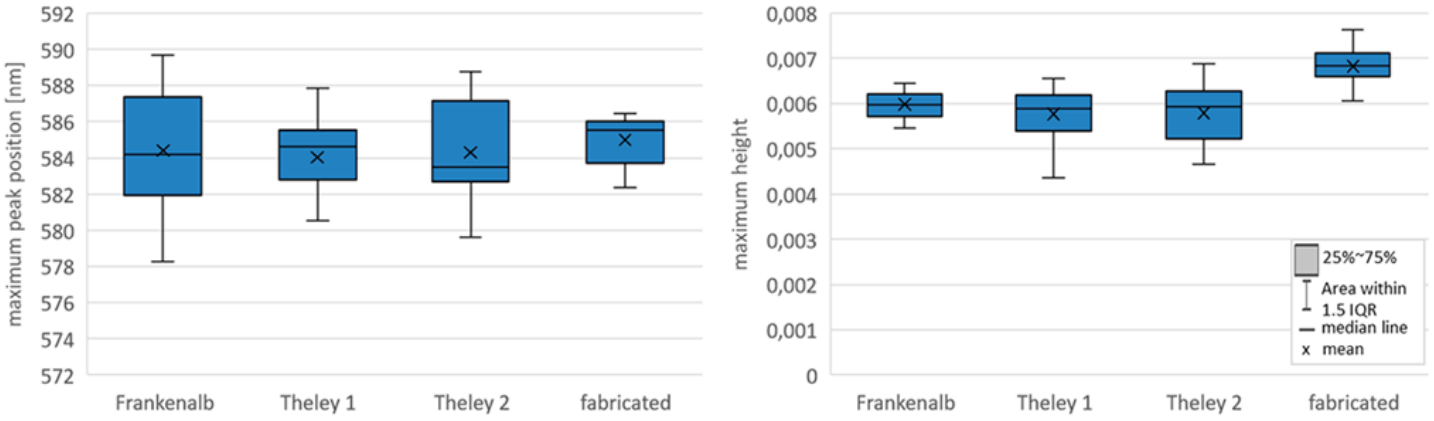

Figure 8

a: Box plots of the red chalk types: distribution of the maximum peak positions of the first derivative (left); distribution of the maximum height of the first derivative (right). Box plot features the median line, mean values, and whiskers indicating 1.5 interquartile range (IQR).

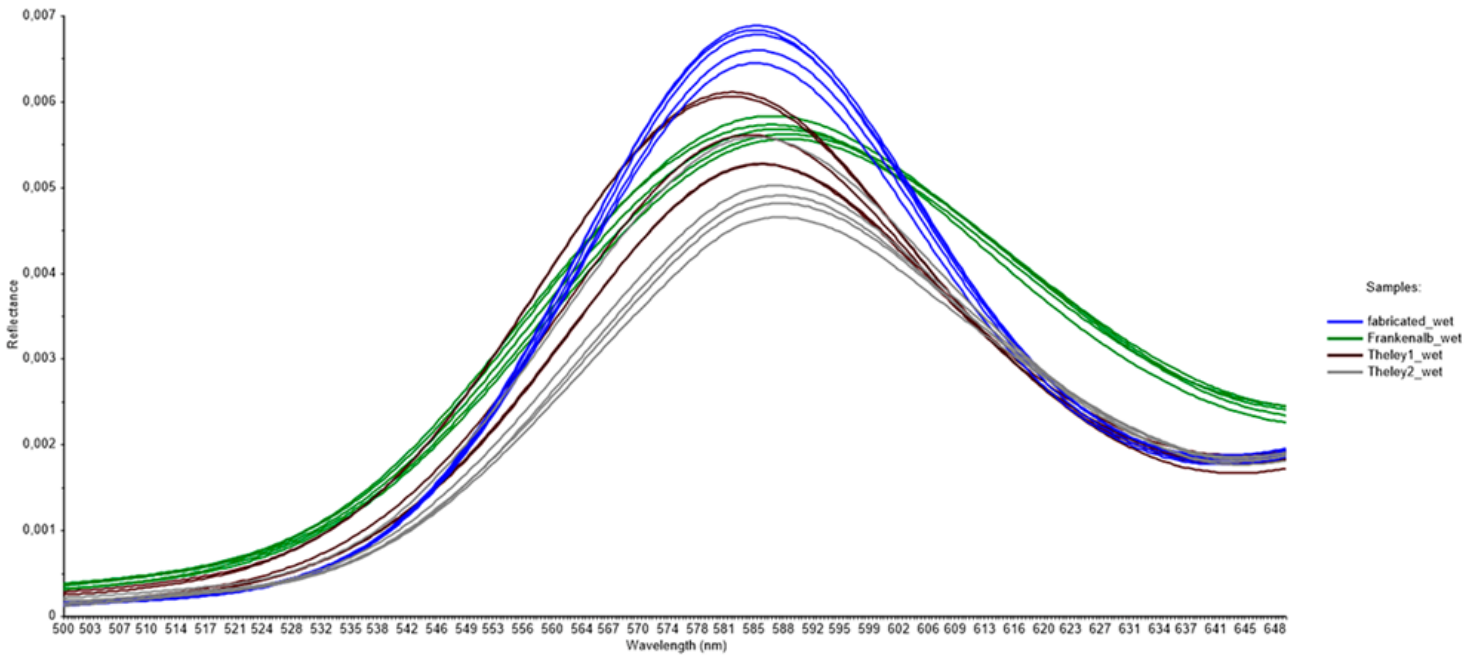

Figure 9

a: First derivative of the FORS spectra between 500–¬650 nm for all chalk types (see Table 1) applied wet on modern paper.

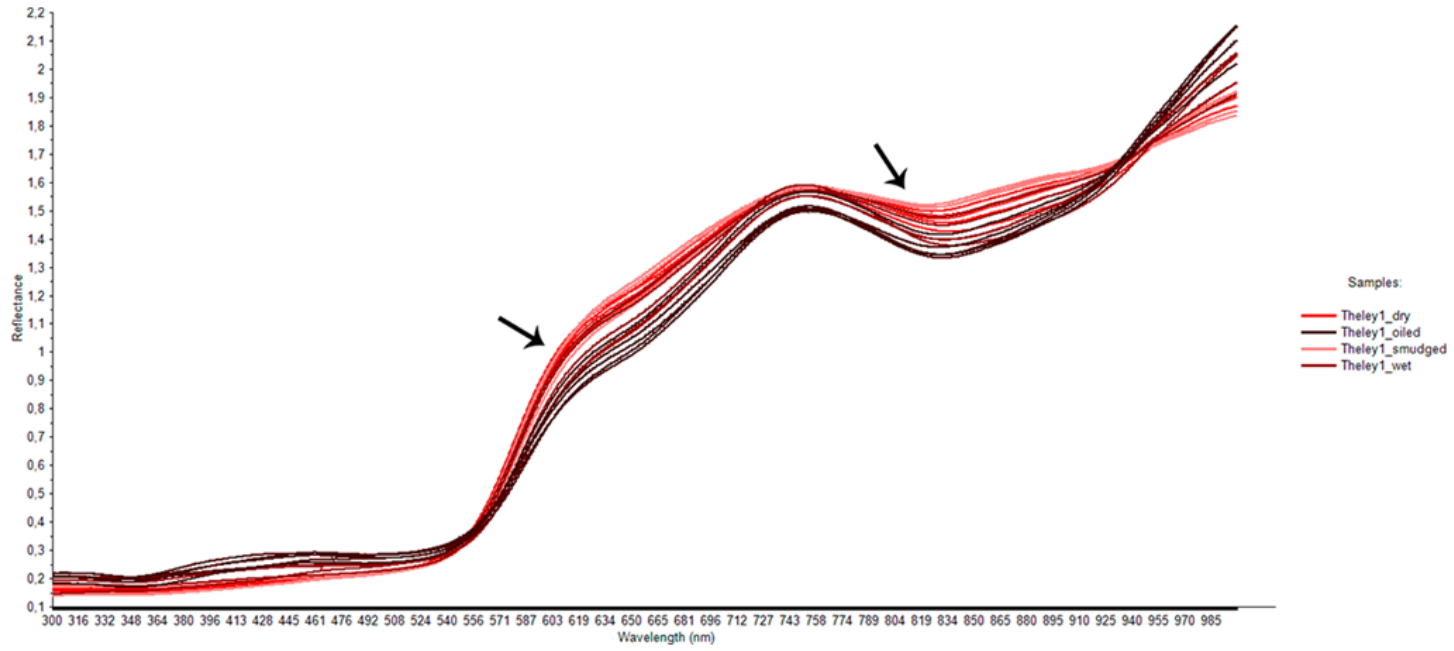

Figure 10

a: FORS reflectance curves in dependence on chalk application technique (Theley1 on modern paper). Arrows mark areas affected by differences between application techniques.

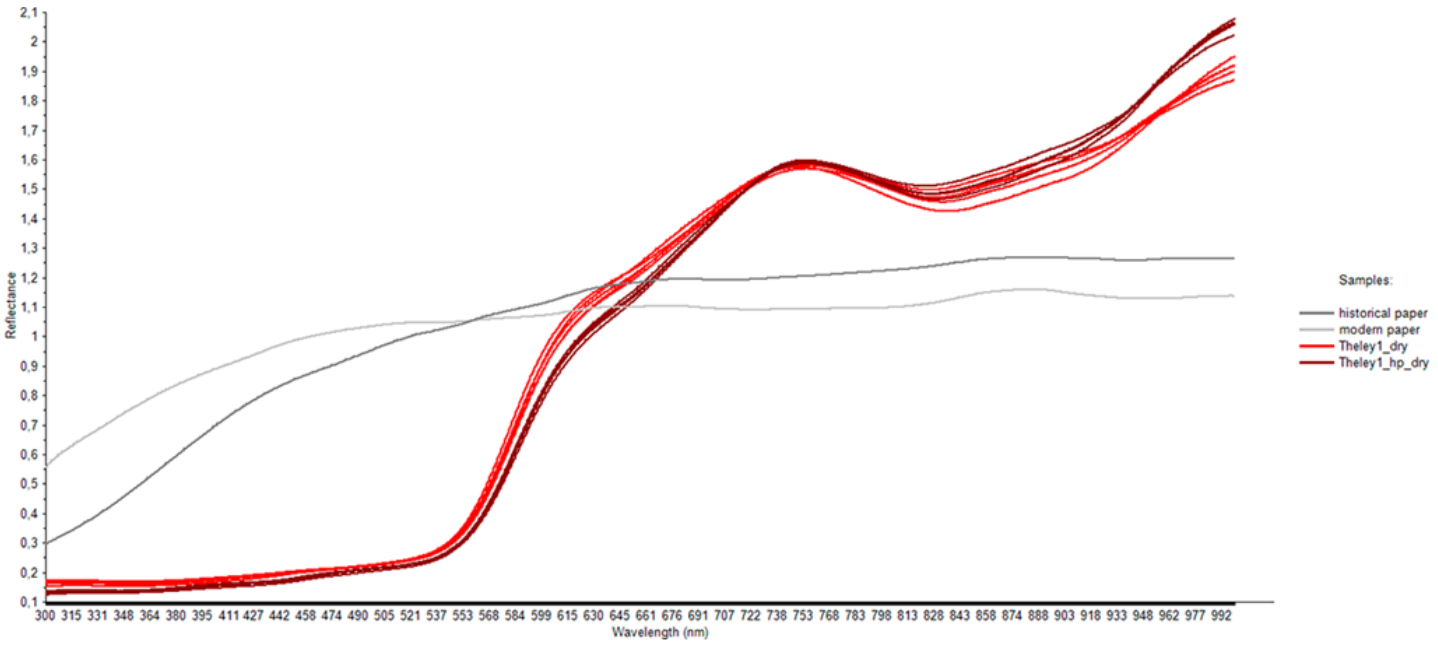

Figure 11

Effect of the paper support (gray) on the reflectance curve for dry chalk applications (Theley1) applied to historical paper (dark red) and modern paper (light red).

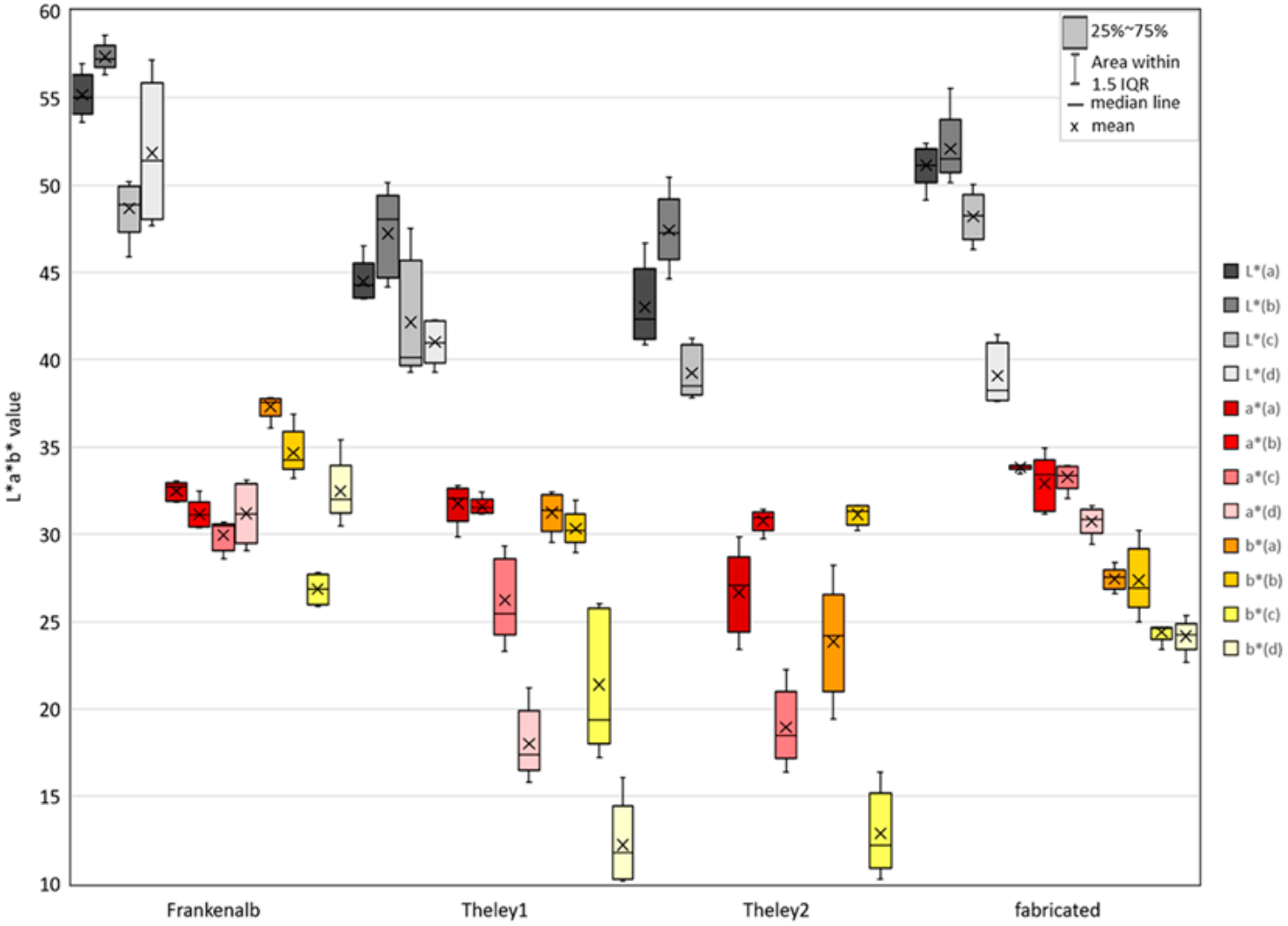

Figure 12

Box plots illustrating variances in the L*, a*, b* values for each chalk type differentiated by application technique (modern and historical papers combined). Application techniques always from left to right: (a)=dry; (b)=smudged; (c)=wet; (d)=oiled.

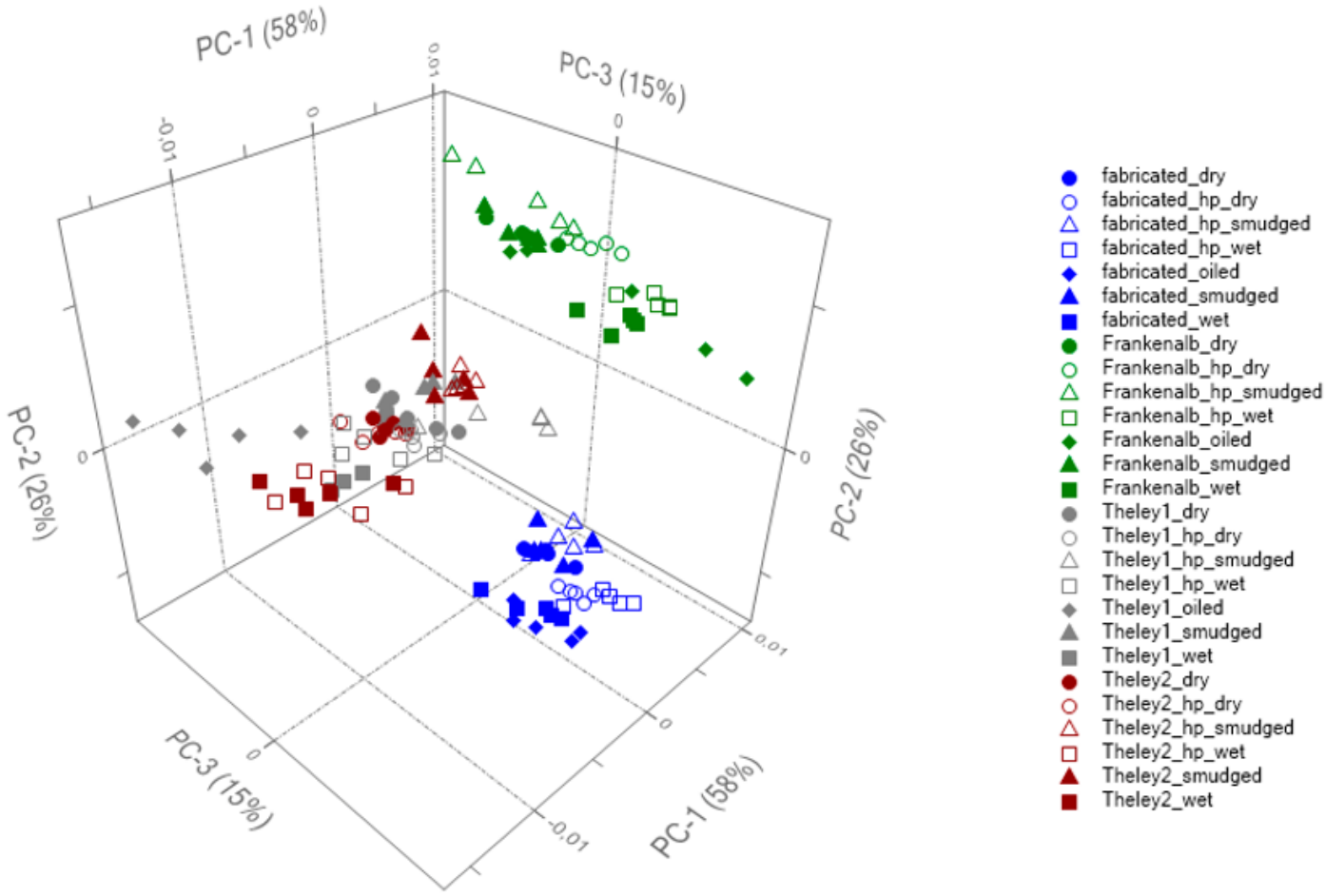

Figure 13

3-dimensional scores plot (PC-1–PC-3). Symbols represent: Color = four tested chalk types (Table 1), shape = application technique; filled = modern paper; unfilled = historical paper.

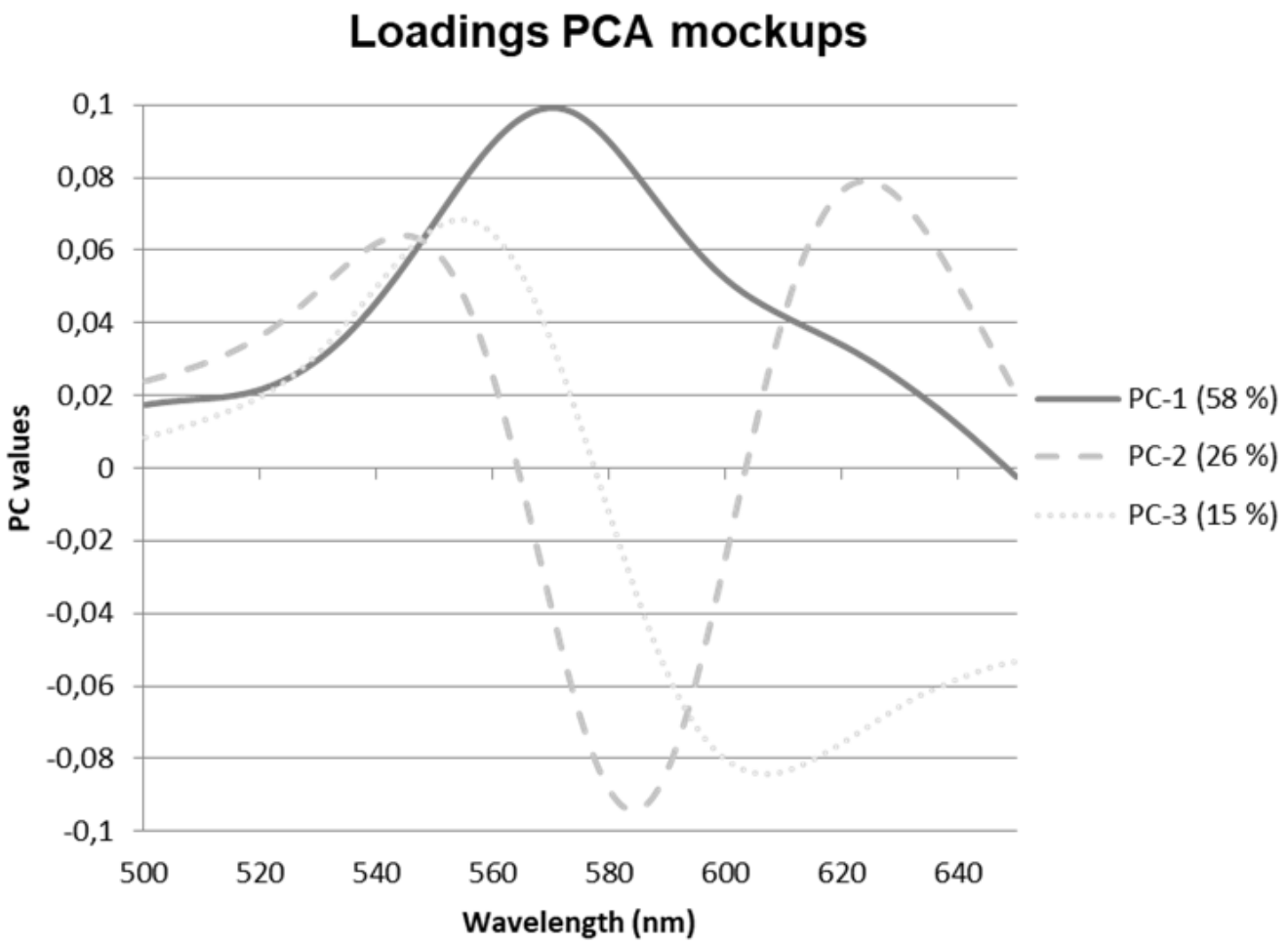

Figure 14

a: Loadings plot for PC-1 – PC-3.

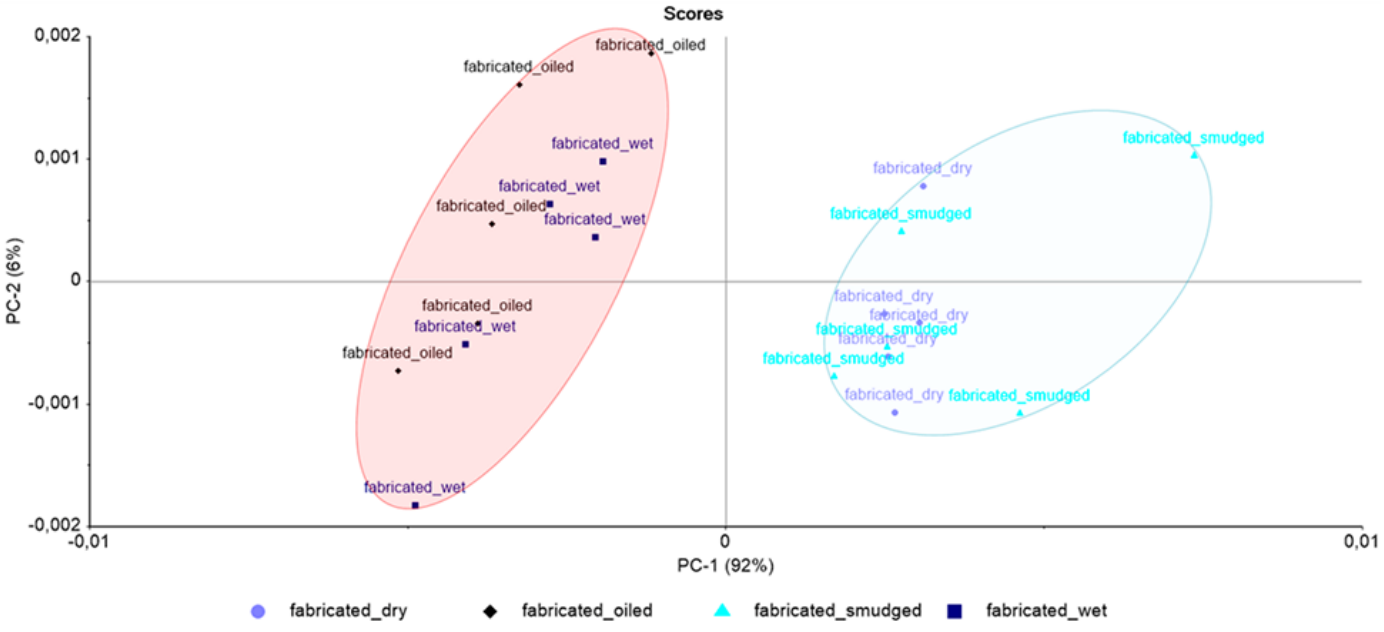

Figure 15

a: Fabricated chalk samples on modern paper divided into two groups along PC-1, according to application technique (red circle = wet techniques, blue circle = dry techniques), circles manually added

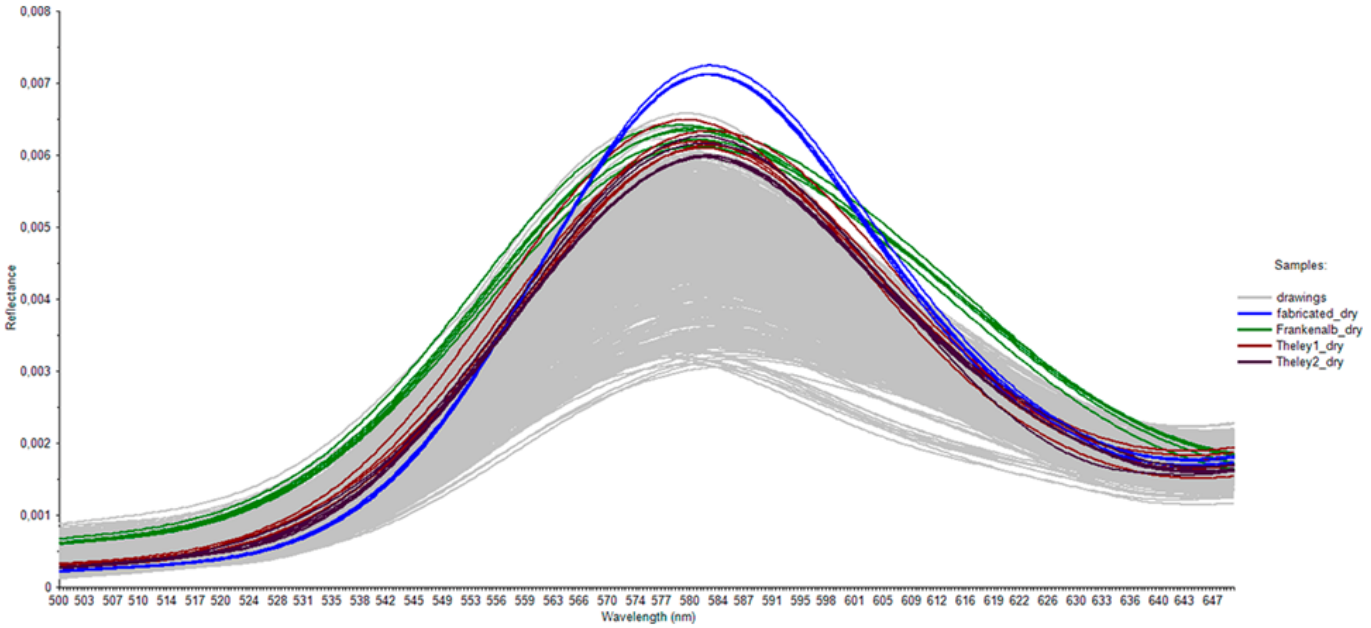

Figure 16

Spectra (first derivative) of 79 original drawings (light gray) and multiple readings of the four reference chalk types (Table 1) applied dry on modern paper.

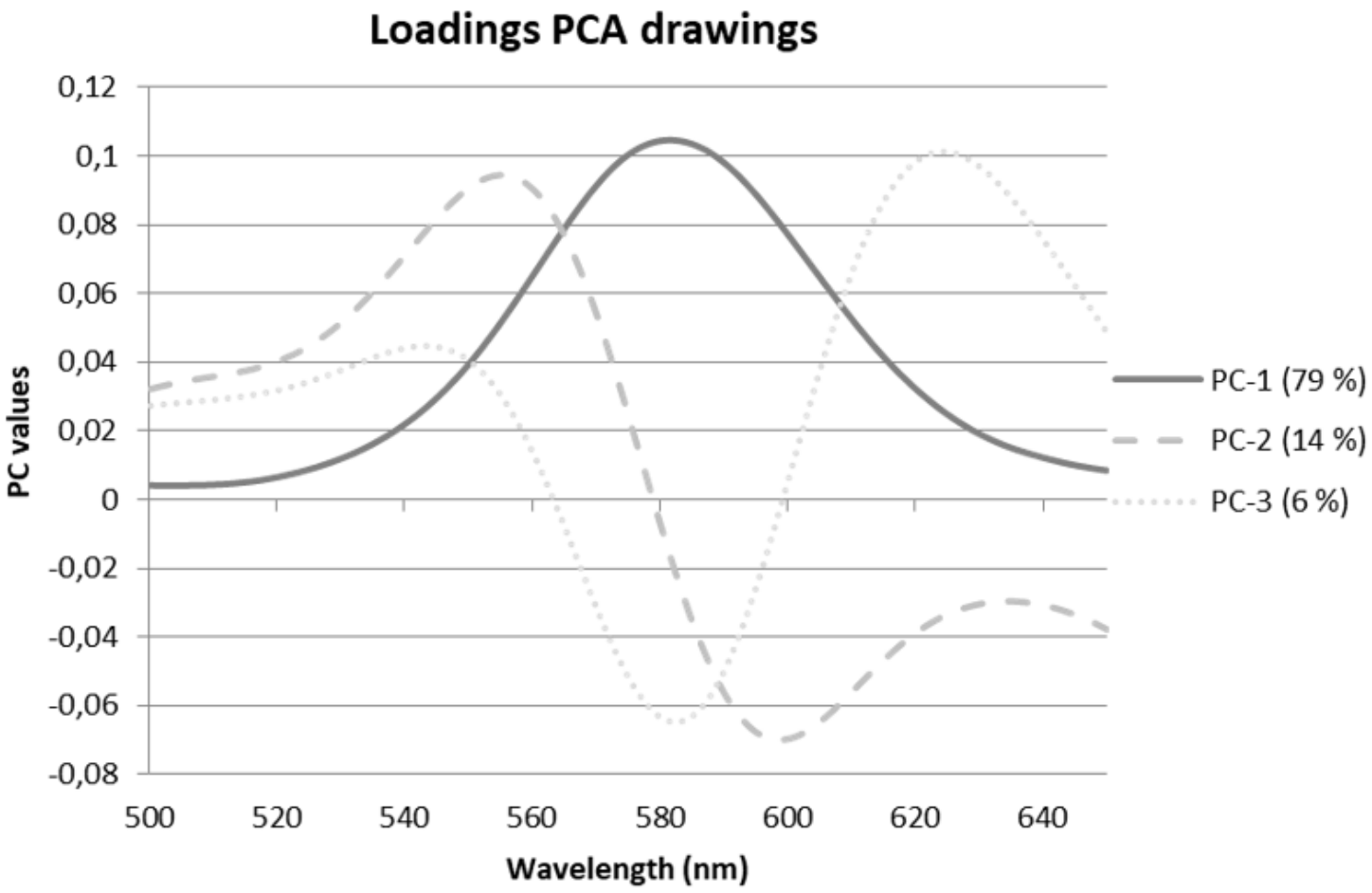

Figure 17

a: Loadings plots for PC-1 – PC-3 for the PCA of the drawings.

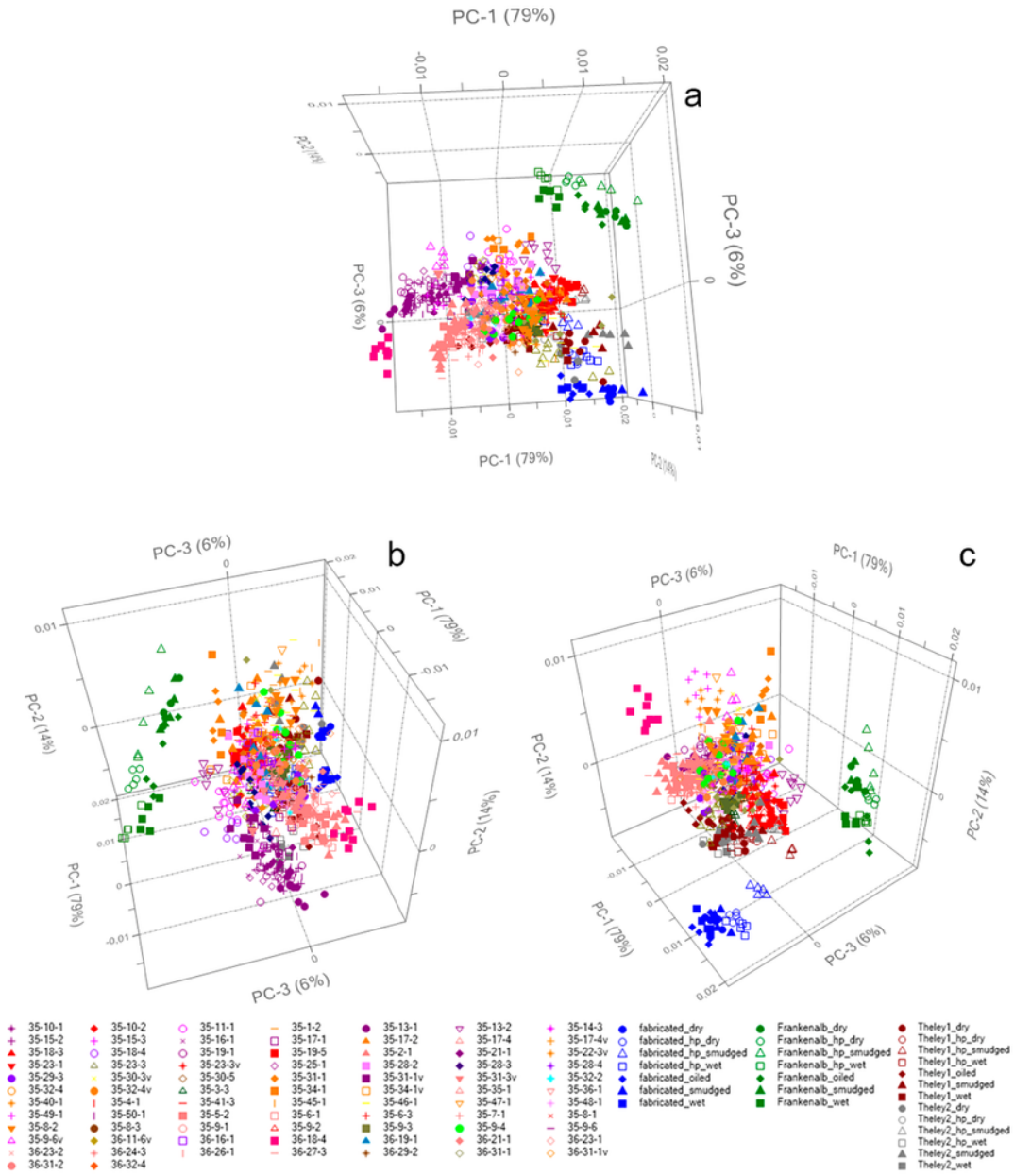

Figure 18

a–c: PCA of original drawings and drawing mockups. Identical colors and symbols interpret the measurements regarding groups of similar red chalks.

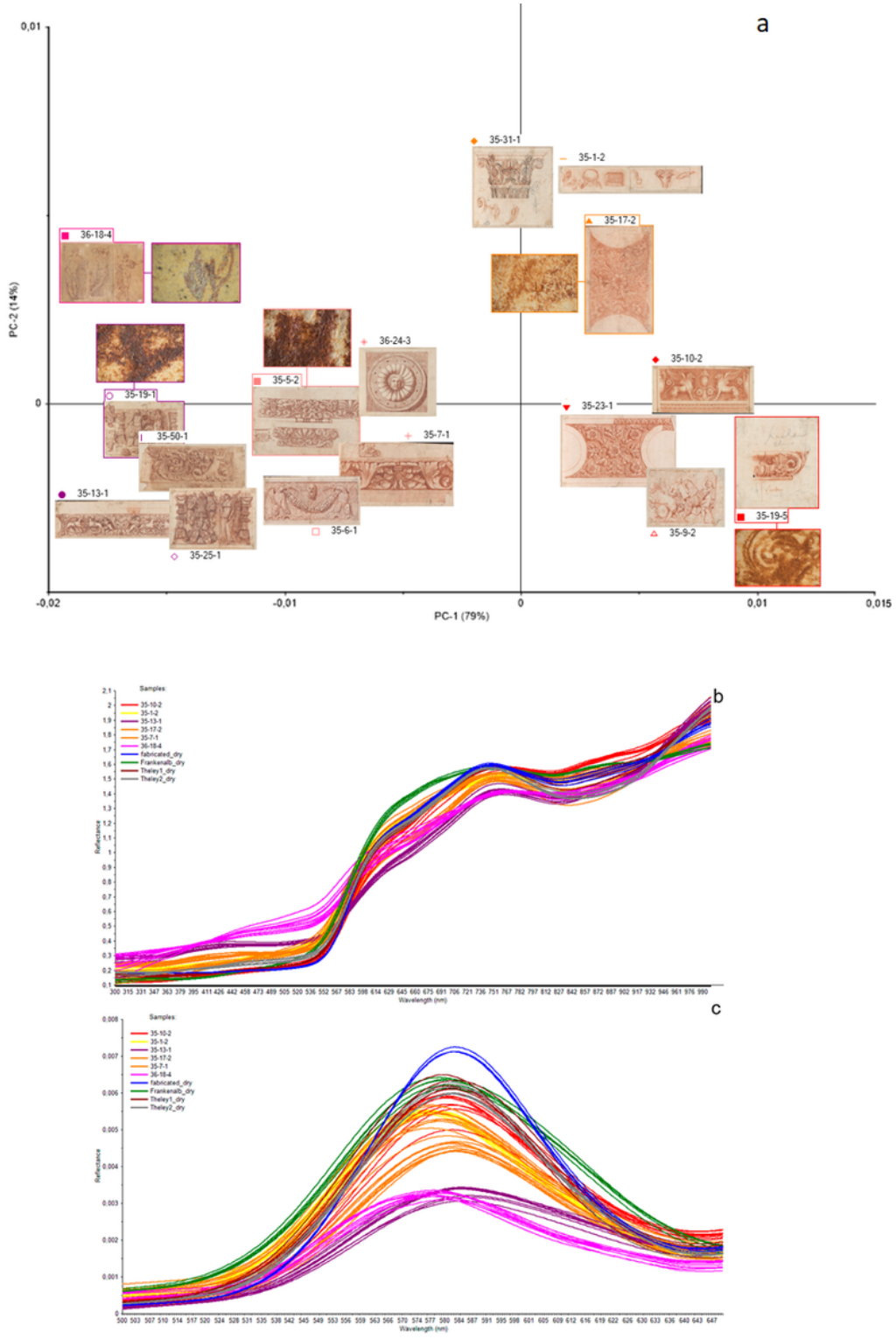

Figure 19

a: Representation of selected original drawings in a PCA score plot matrix that differentiates graduations of red chalk from higher to lesser chromaticity (PC-1) and high to low coverage (PC-2). Drawing 36-18-4 is an outlier, executed on oiled paper. Selected photo macrographs illustrate the appearance of the chalk lines; photographs: Staatliche Kunsthalle Karlsruhe, Maria Krämer. b–c: b (top): FORS reflectance spectra

of selected original drawings and drawing mockups assigned to different clusters via PCA, and c (bottom) their first derivative.

Supplementary Files

This is a list of supplementary files associated with this preprint. Click to download.

- Appendix.docx